CHAPTER ONE

Bending Rigidities of Lipid Bilayers: Their Determination and Main Inputs in Biophysical Studies

Hélène Bouvrais*

Contents

*Corresponding author. Tel.: +45 65504041; Fax: +45 65504048.
E-mail address: helene@memphys.sdu.dk

MEMPHYS—Center for Biomembrane Physics, Department of Physics, Chemistry and Pharmacy, University of Southern Denmark, Odense M, Denmark

Advances in Planar Lipid Bilayers and Liposomes, Volume 15
ISSN 1554-4516, DOI: 10.1016/B978-0-12-396533-2.00006-9

Abstract

Because of the complexity of the biological membranes, artificial membranes are often used as membrane models for biophysical studies. This is especially true for the investigation of the physical properties of the membranes and their elastic deformations. This chapter focuses on the bending rigidities of lipid bilayers, more precisely on their determination and their inputs in biophysical studies. A large variety of techniques is available to determine the bending rigidity: (i) experimental ones such as the flickering technique, the methodologies that respond to a mechanical deformation or the scattering techniques, and also (ii) Molecular Dynamics (MD) simulations. The flickering technique, which is the mostly used method to determine the bending rigidity, consists of first recording the thermal fluctuations of the membrane of giant vesicles by phase contrast microscopy and then measuring the amplitudes of these fluctuations, which depend on both the composition of the lipid bilayer and its environment. Bending rigidity measurements enabled so far to get some important information regarding the temperature effect, the impact of various molecules such as sterols, salts or charged molecules, and the dependence on the chain length and saturation of the lipid. The ability for an amphipathic helix, namely, the magainin peptide, to locally bend the membrane has also been characterized by bending rigidity determination.

1. Introduction

1.1. Membrane Models for Biophysical Studies

1.1.1. Brief overview of the biological membranes

Biological membranes are essential components in living systems, as they serve to compartmentalize cells and organelles, keeping their integrity and maintaining the essential differences between their contents and environments. Plasma membranes provide thus protection from external stresses. These envelopes are also selectively permeable barriers and places of exchange and communication with the external environment. Consequently, the membranes play a major role in the functioning of the cells by regulating, catalyzing, or mediating many biological or biochemical processes through a vast array of membrane-associated proteins, processes such as transport, recognition, immunological response, energy transduction, signaling, and enzymatic activity [1].

To be able to fulfill all the functions mentioned previously, the membrane is complex regarding its composition, structure, and organization. However, all biological membranes have a common general structure: self-assemblies of lipid and protein molecules held together by noncovalent interactions (i.e., hydrogen, hydrophobic, and electrostatic interactions). The plasma membrane of a cell, that is, a mixture of around 50 wt% of lipids, 40 wt% of proteins, and 10 wt% of carbohydrates, is composed of three distinct layers:

(i) the lipid bilayer in the middle, (ii) the glycocalyx facing the extracellular space, and (iii) the cytoskeleton facing the cytosol (Fig. 1). The lipid bilayer, which serves as a relatively impermeable barrier to the passage of most water-soluble molecules, is a self-assembling of several kinds of lipids, in which are inserted proteins, that mediate most of the specific functions of the membrane. In the extracellular side of the membrane, the lipid bilayer is covered with carbohydrate residues coming from lateral tails of either glycolipids or glycoproteins. While the glycocalyx, meaning literally "sugar coat," forms a protective layer for the cell, which is important for the adhesion and cell recognition, the cytoskeleton (from the greek, cyto = cell, skeletos = dried up) is a tridimensional network of proteic filaments found inside the cell. This dynamical structure is coupled to the membrane, allowing to keep or change the cell shape. The cell motility and the motion of the internal organelles are thus done through the cytoskeleton.

Lipids (from the greek, lipos = fat) are a special category of amphiphilic molecules, generally composed of a polar head group and two hydrophobic tails [2–4]. A huge variety of lipids exists in cells according to the length and degree of saturation of the tails and according to the kind of head groups. Usually, the tails contain between 14 and 24 carbon atoms, and one tail has one or more double bonds, while the other tail does not. One of the main classes of lipids is the glycerophospholipids, which have two fatty acids bound to the first and second position of a glycerol molecule and a phosphate-containing head group bound to the third position. Lipids typically self-assemble in water to form a bilayer, which can be defined as a bidimensional thin fluid film above a given temperature, T_m (melting temperature). This thin film provides an effective barrier, with a typical thickness of only

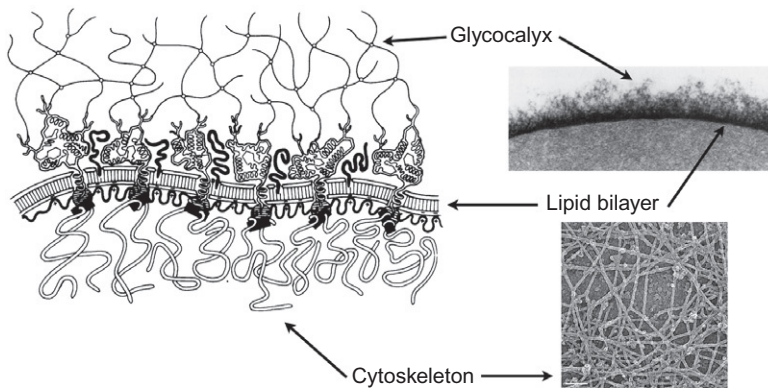

Figure 1 Sketch and electronic microscopy images of the plasmic membrane with the three layers: lipid bilayer, glycocalyx, and cytoskeleton, adapted from Ref. [2]. Notice that the lipid/protein bilayer and the glycocalyx are enlarged in thickness by a factor of about 300 compared to the macromolecular networks.

two lipid molecules (i.e., about 5 nm) and an intermolecular distance of 0.5 nm. Variations in the relative proportions of lipids are observed among the different membranes, such as erythrocytes, plasma, endoplasmic reticulum (ER), Golgi, lysosome, nuclear membrane, mitochondria, and neurons, where the main lipids are phospholipids, cholesterol, and glycolipids (see Ref. [5] for examples of lipid composition).

While lipids play a crucial role in the compartmentalization, proteins are also important in the membranes as they carry out most of the specific functions. The amounts and types of proteins in a membrane are highly variable, with, for instance, the mass ratio between proteins and lipids that ranges between 0.25 (lung surfactant) and 4 (purple membrane of halobacteria). Typically, biological membranes display a protein–lipid ratio of approximately one; this includes the extra-membrane parts of the proteins and the surface-associated proteins. Some membrane proteins serve to transport specific molecules into or out of the cell (for instance, Na,K-ATPase is an enzyme that pumps $2K^+$ in and $3Na^+$ out of the cell while one molecule of ATP is hydrolyzed), whereas others are enzymes that catalyze membrane-associated reactions. Furthermore, some membrane proteins are structural links that connect the plasma membrane to the cytoskeleton and/or either the extracellular matrix or an adjacent cell. Last but not least, others play the role of receptors for receiving and transducing chemical signals in the cell environment.

Membrane carbohydrates usually compose between 2% and 10% of membrane total weight. All eukaryotic cells have carbohydrates on their surface, both as oligosaccharide and polysaccharide chains covalently bound to membrane proteins (glycoproteins) or as oligosaccharide chains covalently bound to lipids (glycolipids).

To reach the current picture of the biological membrane, the history of membrane models has involved several steps, starting with the important discovery from Gorter and Grendel [6] in 1925 (cell membranes made of two thin monolayers), continuing with the different models of Danielli and Davson [7] in 1935 (membrane described as a sandwich of lipids covered by proteins on the both sides) and of Robertson [8] in 1957 ("unit membrane"), and the most famous one in 1972, namely, "the mosaic fluid model" from Singer and Nicolson [9]. Figure 2 sketches an elaborated membrane model taking into account membrane undulations, lateral heterogeneity, lipid domain formation, and thickness variations in the lipid bilayer. This current model captures the last discoveries of the membrane history from Israelachvili [10] and from Mouritsen and Bloom [11] with the "mattress model", and the raft hypothesis [12–14].

1.1.2. Artificial membranes as membrane models

As described previously, biological membranes are complex systems composed of a rich variety of lipids, which need to be simplified, so that for instance biophysicists can understand and investigate their properties.

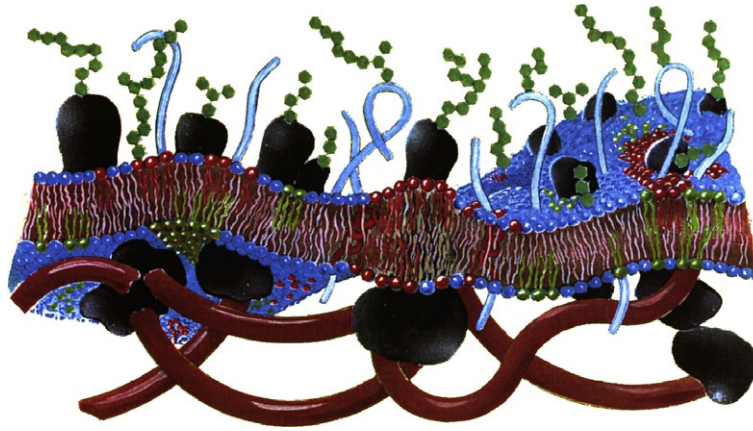

Figure 2 Sketch of the biological membrane. Notice that the different membrane components are not drawn to scale and that structural details of the proteins have been omitted to capture many different features in the same illustration (Courtesy from Ole G. Mouritsen from MEMPHYS).

For the biophysical characterization of biological membranes, two model systems have in the past been particularly successful. One is the supported membrane system, which consists of a solid support (mostly polished glass or mica surface) and on top of it one or several double layers of lipids [15,16]. This system is usually called supported lipid bilayers (SLBs). The other model system, namely, the free standing membranes, involves various kinds of vesicles, which can differ according to their size and lamellarity. However, for the characterization of a single membrane, the first choice for the free standing membrane is the giant unilamellar vesicle (GUV), a closed lipid bilayer system with a diameter well above the optical resolution limit, that is, from several microns up to hundreds of microns [17]. Both systems (SLBs and GUVs) use lipid bilayers as a model to understand, for instance, the topology, shape fluctuations, phase behavior, permeability, fission and fusion of biological membranes.

The simplest cell model is the lipid vesicle, also called the liposome, which can be found with various morphologies [18,19]. Liposomes are spherical, self-closed vesicles of colloidal dimensions (in the range from 20 nm to 100 μm), in which a lipid bilayer sequesters part of the solvent into their interior. In the case of one bilayer encapsulating the aqueous core, one defines either small, large, or giant unilamellar vesicles (SUVs, LUVs, or GUVs, respectively), while in the case of many concentric bilayers, one speaks of large multilamellar vesicles (MLVs) with their onion-like structure.

GUVs with a size close to one of the cells are really fascinating membrane model systems [20–22], which were initially reported as alternative

membrane model systems by Reeves and Dowben [23] in 1969. Since then, the number of published studies referring to GUVs has constantly grown with specially a dramatic increase noticed in the past 15 years, illustrating that giant vesicles have become very popular objects useful for physicists and biophysicists as membrane model systems or as passive objects for method developments [24–31]. GUVs are perfect candidates as membrane models because of their direct and easy observation by optical microscopy, as the dimensions of GUVs (mean diameter around 25 μm) are higher than the intrinsic resolution limit of light microscopy related techniques (∼250 nm radial). Besides, the average size of GUVs is similar to that of a variety of cells, which allows to perform experiments at the level of single vesicles on the same size scale (curvature) as natural membrane systems. Another advantage in using giant vesicles as model systems is the ability and easiness to control the molecular composition of the membrane as well as the environmental conditions. Thus, while the production of giant vesicles composed of a single lipid species or a mixture with a few components was typically done for many years [23,32,33], it has been possible only recently to form giant vesicles from natural lipid extracts [34–37] and native membranes [35,38–40], which has given even more credit in using GUVs as membrane models.

A variety of techniques exists for the formation of GUVs [17,23,32,33,35,41–43] and there is no general agreement in the experimental protocol required to obtain GUVs. This lack of consensus might be due to the fact that the mechanism explaining giant vesicle formation still remains unclear. It is worth noticing that most of these methods are based on two main experimental protocols: the electroformation method (or electro-swelling method) introduced by Angelova and collaborators [32,33] and the spontaneous swelling method (or gentle hydration method) originally described by Reeves and Dowben [23]. Recently, the electroformation method has been improved by Pott *et al.* [44] so that it can be used with complex membrane composition, that is, in the presence of proteins and with various buffer solutions, including physiologically relevant conditions. These improvements of the electroformation method were necessary so that the membrane composition and aqueous environments could be adjusted to the purpose of the study, in order to broaden the use of GUVs for biology or biochemistry. The first major improvement was the use of aqueous vesicle suspensions (either LUVs or SUVs, obtained from extrusion [45–47], reverse phase evaporation (REV) [48], or sonication [49–51]) as deposits instead of lipids dissolved in organic solvent, which allows to work on complex membrane composition, with mixtures of lipids and proteins [52]. Thus, this method, originally developed for single phospholipid species, has been used with success to prepare GUVs from native biological membranes, for example, from ghosts [39] or from pulmonary surfactants [35]. The insertion of fragile proteins, such as Ca^{2+}-ATPases, in GUVs with recovery of their activity has been another great illustration of the usefulness of aqueous vesicle

suspensions as deposits [41]. The second major improvement of the electroformation method was the capacity to produce GUVs under physiologically relevant conditions (pH and salinity). For that, the parameters of the electric field had to be adapted to the medium, for example, salt concentration or pH. Thus, a frequency change of the electroformation parameters from 10 to 500 Hz enabled to form GUVs for low salinity (pure water or less than 10 mM for total salt concentration) and high salinity (total salt concentration between 100 and 150 mM), respectively. Consequently, due to these two improvements of the protocol, it is now possible to produce GUVs from various types of liposomes and proteoliposomes and further under physiologically relevant conditions, which allows to use the giant vesicles as isolated and easily visualized objects for a variety of biologically relevant purposes.

1.2. Physical Properties of the Membranes and Their Elastic Deformations

At the macroscopic scale, namely, at observed distances large compared to molecular sizes, the membrane is a continuous medium and can be considered as an infinitely thin surface, that is, a material with specific properties. These macroscopic properties (bending rigidity, stretching elasticity, and membrane viscosity) are linked to the microscopic structure of the membrane described previously and will depend mainly on the membrane thermodynamic state and composition.

The membrane collective motions lead to three typical elastic deformations: (i) area expansion/compression, (ii) shearing deformation, and (iii) bending deformation, as schematically described in Fig. 3. The membrane responses to these various deformations are characterized by the following constants: shear elastic modulus μ, area compressibility modulus K_a, bending rigidity κ, and Gaussian curvature modulus k_G.

As, at physiological temperature, most lipid membranes are fluid, they cannot sustain shear forces ($\mu = 0$), while below the main phase transition temperature T_m of the lipids, membranes crystallize and, thus mechanically, the bilayer acquires a nonzero shear elasticity.

The possible expansion–compression deformation appears to be very limited for the lipid bilayer. As described by Eq. (1), the stretching elastic energy per unit area, E_{exp}, depends on the increase or decrease of the relative area $\Delta A/A_0$, according to the well-known Hooke's law for an elastic spring. Area changes are found not to be able to exceed 5% so that, above a critical lysis tension (around 10^{-3} N/m), hydrophilic pores will be formed in the membrane until its complete destruction [53].

$$E_{exp} = \frac{1}{2} K_a \left(\frac{\Delta A}{A_0} \right)^2 \tag{1}$$

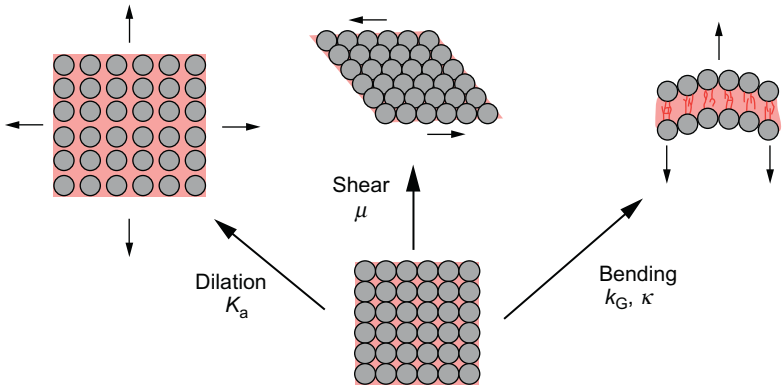

Figure 3 Schematic representation of three classical modes of bilayer deformations: dilation, shear, and bending, with the associated constants characterizing the membrane response to these deformations, namely, K_a, μ, k_G, and κ.

with $\Delta A = A - A_0$, where A_0 and A are the equilibrium and deformed area of the membrane, respectively.

The bending deformation, whose energy per unit area, E_{bend}, is described according to Helfrich by Eq. (2), plays a major role in the membrane shapes as a lipid film is extremely thin and thus exerts weak opposition to out of plane bending [54]. The membrane bending is characterized by three phenomenological parameters: (i) the bending elastic modulus, κ, which contains all the microscopic details of the bilayer (rigidity and length of the lipid tails, nature of interactions between polar heads, etc.), (ii) the Gaussian elastic modulus, k_G, which measures the elastic energy associated to the intrinsic curvature, and (iii) the spontaneous curvature, C_0, illustrating an eventual asymmetry in the lipid composition of the two leaflets or the shape adopted by the bilayer in the absence of constraint, while C_1 and C_2 are the principal curvature axes of the membrane describing the local curvature.

$$E_{\text{bend}} = \frac{1}{2}\kappa(C_1 + C_2 - C_0)^2 + k_G \cdot C_1 C_2 \tag{2}$$

Table 1 displays some typical values of the elastic moduli listed previously for different kinds of membranes. For comparison, known values of these constants for synthetic materials exhibiting the same size and topology, such as brass, polyethylene, and rubber, are also given in Table 1. These comparisons underline that cell membranes have remarkable properties, as they appear to be extremely soft with respect to bending and shearing, while they are laterally incompressible.

Table 1 Elastic moduli of various kinds of materials: μ the shear modulus, K_a the compression modulus, and κ the bending modulus, adapted from Ref. [55]

Materials	μ (J/m^2)	K_a (J/m^2)	κ (J)
Brass	110	100	10^{-15}
Polyethylene	5	5	5×10^{-17}
Rubber	0.05	0.06	5×10^{-20}
Red blood cell	6×10^{-6}	0.45	7×10^{-20}
DMPC	0	0.145	1.2×10^{-19}
POPC	0	0.213	1.58×10^{-19}
POPC with 30 mol% Chol	0	0.354	3.57×10^{-19}

When the lipid membrane is above the main phase transition temperature, that is, when the membrane is fluid ($\mu=0$), the two relevant contributions for the mechanics of lipid bilayers are the compression and bending ones. The elastic free energy, $\mathcal{H}$, that describes membrane deformations, can thus be written according to Eq. (3).

$$\mathcal{H}=\frac{A_0}{2}K_{\mathrm{a}}\left(\frac{\Delta A}{A_0}\right)^2+\frac{1}{2}\kappa\int_A \mathrm{d}A(C_1+C_2-C_0)^2+k_{\mathrm{G}}\int_A \mathrm{d}A C_1C_2 \qquad (3)$$

The Gauss–Bonnet theorem in differential geometry is an important statement about surfaces, that connects their geometry (in the sense of curvature) to their topology [56,57], namely, that the integral of the Gaussian curvature over a compact surface S is a topological invariant as stated by Eq. (4). Notice that a compact surface in a topological sense means a closed and limited surface, and that genus in Eq. (4) is the number of handles of a surface. Thus, the Gaussian curvature contribution does not change for a vesicle subject to thermal fluctuations, as it can be modeled as a compact surface.

$$\int_S \mathrm{C}_1\mathrm{C}_2 dA=4\pi(1-\mathrm{genus}) \qquad (4)$$

Therefore, the only relevant elastic constants left associated to Eq. (3) are the area compressibility modulus K_a found to be around 0.1–1 J/m^2 (equivalent to $\sim10^7$–10^8 $k_BT/\mu\mathrm{m}^2$) and the bending elastic modulus κ that is of the order of 10^{-19} J (i.e., in the range 10–100 k_BT). The order of magnitude of the membrane bending rigidity suggests that changes in the conformational fluctuations of the lipid vesicles can be induced simply by thermal energy, that is, without any external energy input. Thus, when no mechanical stretching of the membranes occurs, the first term of the elastic free energy in Eq. (3) can be omitted.

Taking into account these two last comments (i.e., omission of both the Gaussian curvature and the expansion–compression contributions), the Hamiltonian of Canham–Helfrich defined by Eq. (5) is obtained to describe the thermally induced membrane shape fluctuations.

$$\mathcal{H} = \sigma A + \frac{1}{2}\kappa \int_A dA (C_1 + C_2 - C_0)^2 \tag{5}$$

where σ (J/m^2) defines the effective surface tension that depends on the total area and the volume of the vesicle.

For a complete description of the membrane, some dynamical coefficients can also be mentioned. For instance, the presence of the two monolayers constituting the lipid bilayer, which may slip with respect to each other, has to be considered. The membrane opposes to this motion with a friction force, that is proportional to the coefficient of intermonolayer friction, b. Besides, one has also to account for viscous dissipation from water hydrodynamic movements, mean surface convection of the bilayer, and differential flow between monolayers, characterized by different viscosity coefficients η depending on the composition of the aqueous environment and the lipid bilayer for instance.

2. Methods for the Determination of the Bending Rigidity

Various experimental techniques exist to measure the bending elastic modulus, also called bending stiffness modulus, curvature elastic modulus, or bending rigidity. As lipid bilayers are as thin as two lipid molecules, their membrane rigidity is extremely small, typically between 10 and 100 times the thermal energy $k_B T$, and this parameter is thus difficult to measure experimentally. The available experimental techniques can be classified into three categories: (i) techniques based on the analysis of the thermal fluctuations by using the dependence of thermal undulations on the membrane bending rigidity, (ii) techniques that study the elastic responses to a mechanical deformation (micropipette, electric field, magnetic field, etc.) by measuring the force needed to actively bend the membrane, and (iii) scattering techniques. The notations used for this parameter will be k_c or κ depending on the technique performed. The bending elastic modulus reflects the resistance or the energy cost to bend a surface: the more difficult it is to bend a membrane, the higher the bending rigidity will be. The bending rigidity is closely related to the composition and environment of the vesicle, namely, the chemistry of the lipids, the temperature, the nature of the structural phases, the aqueous solution composition, etc.

The first measurement of the bending elastic modulus was made in 1975 by Brochard and Lennon [58] for red blood cell (RBC) membranes, studying the flickering of these cells. The flickering phenomenon was observed originally in 1890 by Browicz [59] but understood only nearly one century later by Brochard and Lennon [58], who attributed these observations to the thermal fluctuations of the membranes, induced by the Brownian motion of the water molecules surrounding the membrane. The flickering phenomenon of RBCs consists of a modulation of transmitted light due to changes of cell thickness and related changes of light absorption. This first measurement of k_c modulus for RBCs membrane led to values between 0.13×10^{-19} and 0.3×10^{-19} J [58].

2.1. Flickering Technique

The determination of the bending elastic modulus of fluid lipid membranes by observation of thermally induced shape undulations of vesicles has become a well-established experimental technique, since it has been argued in 1975 that the flickering phenomenon of RBCs can be explained in terms of thermal conformational fluctuations. Thermal fluctuations in shape are observable by light microscopy, making the Vesicle Fluctuations Analysis (VFA) one of the obvious techniques to determine the bending rigidity. This method, typically termed "flicker spectroscopy" or "flickering technique," consists of monitoring by light microscopy the membrane fluctuations of a vesicle as a function of time and measuring the amplitudes of these fluctuations.

Bending rigidities have since then been obtained from flickering of tubular vesicles [60–62], vesicle portions [63], and quasispherical vesicles [64–87].

2.1.1. For tubular vesicles

The first flickering studies were mainly performed on tubular vesicles.

In 1976, Servuss *et al.* [62] observed under microscope the fluctuations of tube-like vesicles considered as one-dimensional objects, whose curvature elastic modulus was expressed via the curvature modulus of the membranes and the radius of the tube. The bending elastic modulus of egg-yolk lecithin (EYPC) was found to be equal to $(2.3 \pm 0.3) \times 10^{-19}$ J.

In 1985, Beblik *et al.* [60] studied the bending modulus for a few synthetic lipids, whose values are displayed in Table 2.

Schneider *et al.* [61] also used tubular vesicles and video imaging technique to determine the bending elastic modulus, by measuring the correlation function of the displacement of the middle point of the tube with respect to the middle point of the segment connecting the ends of the tube. Their obtained values of k_c for egg phosphatidylcholine (EPC) were in the range from 1×10^{-19} to 2×10^{-19} J.

Table 2 Bending rigidities of various synthetic lipids obtained by studying the flickering of tubular vesicles [60]

Lipid	k_c ($\times 10^{-19}$ J)
DMPC (26 °C)	2.4 ± 0.4
DPPC (44 °C)	2.0 ± 0.4
DSPC (56.5 °C)	1.8 ± 0.3
Egg-lecithin (24 °C)	2.0 ± 0.5

Table 3 Bending elastic moduli of synthetic lipids obtained by studying the thermal fluctuations of membranes straight sections in pure water [63]

Lipid	k_c ($\times 10^{-19}$ J)
DGDG (20 °C)	0.20 ± 0.06
DMPE (60 °C)	0.70 ± 0.10
EYPC (20 °C)	0.80 ± 0.20

2.1.2. For vesicle portions

Nearly straight sections of fluctuating membrane contours have also been recorded and Fourier analyzed.

The bending elastic modulus was thus derived from undulations of extended membranes in pure water, and calculations of the mean squares of the fluctuation Fourier amplitudes $\langle {A_{q_x}}^2 \rangle$ gave access to the k_c modulus according to Eq. (6).

$$\left\langle A_{q_x}^2 \right\rangle = \frac{k_B T}{2\sqrt{A} q_x^3 k_c} \tag{6}$$

with A the area of the membrane piece and q_x the wavelength vector.

The data obtained by Mutz *et al.* [63] using this approach are displayed in Table 3.

2.1.3. For quasispherical vesicles

Most of the flickering measurements to get the κ modulus have been performed on GUVs, that have to be quasispherical to fulfill the conditions of the different theoretical models developed so far.

In 1984, Schneider *et al.* [86] studied the bending rigidity for egg-yolk lecithin with quasispherical vesicles this time and obtained a value of $(1.5 \pm 0.5) \times 10^{-19}$ J by measuring the correlation function. They used a new theoretical model by looking at the temporal autocorrelation function of the fluctuations of two diameters situated at 90° from each other.

Engelhardt *et al.* [69,85] applied the theory of Schneider and did the Fourier analysis of the thermally excited surface undulations for all the contour decompositions. The shape changes expressed by Eq. (7) were done in terms of a Fourier expansion of the contour.

$$R(\phi) - R_0(\phi) = \sum_q u_q \exp(-iq\phi) \tag{7}$$

with $R(\phi)$ the instantaneous radius, $R_0(\phi)$ the average contour, ϕ the rotational angle, and q the wave vector.

Therefore, by measuring the mean square amplitudes $\langle u_q^2 \rangle$, they could obtain the curvature elastic constant, k_c, according to Eq. (8).

$$k_c = N(q) \frac{k_B T R^2}{\langle u_q^2 \rangle} \tag{8}$$

with R the average radius of the vesicle.

They expected more precision with their approach than the one of Schneider. However, the measurements made on a few synthetic phospholipids did not show any major differences between the lipid species: for DMPC at 26 °C the bending modulus was equal to $(0.35–0.65) \times 10^{-19}$ J, for DMPC/DPPC 1:1 at 36 °C k_c was found to be $(0.38–0.49) \times 10^{-19}$ J, and for DMPC + 6 mol% of cholesterol at 29 °C $k_c = (0.28–0.37) \times 10^{-19}$ J.

Duwe *et al.* [68] also used the Fourier analysis of thermally excited membrane undulations to obtain the bending elastic modulus of different systems, whose results are displayed in Table 4.

In 1987, Bivas *et al.* [64] measured the k_c modulus by observing the thermal fluctuations of quasispherical vesicles under a microscope equipped with the Nomarski Differential Interference Contrast. They introduced the angular correlation function of thermal shape fluctuations to measure

Table 4 Bending rigidities obtained by Fourier analysis of thermally excited membranes undulations of giant vesicles [68]

Lipid	k_c ($\times 10^{-19}$ J)
DMPC (30 °C)	1.15 ± 0.15
DMPC/cholesterol: 80/20 (30 °C)	2.1 ± 0.25
DMPC/cholesterol: 70/30 (30 °C)	4.0 ± 0.80
Egg-PC	1.15 ± 0.15
DMPC/1,2di(5C_1-16:0)-PC: 1/1	1.7 ± 0.2
Galactosyldiglyceride	$0.15 - 0.4$
Erythrocyte	$0.3 - 0.7$

the bending elastic modulus of egg-yolk lecithin and found a value of $(1.28 \pm 0.25) \times 10^{-19}$ J.

In 1989, Faucon *et al.* [70] used several new parameters and procedures to study the thermal fluctuations of GUVs in order to obtain the bending elastic modulus. (i) The reduced membrane tension was introduced in the Helfrich equation for the conservation of both the vesicle volume and the membrane area. (ii) To improve the statistics for the evaluation of the bending elastic modulus, a large number of contours (several hundreds) from vesicles observed by phase contrast microscopy were considered. (iii) The white noise on the Fourier amplitudes was eliminated by using the angular autocorrelation function previously introduced by Mitov *et al.* [88]. (iv) The video integration time (t_s) of 40 ms was taken into account by implementing a corrector factor of the amplitudes as expressed in Eq. (9). This corrector factor was required because of a smearing of the quickly moving part of the contours, consequence of the way the image was formed by the microscope, namely, by an accumulation between two successive scans of 40 ms.

$$B'_n(t) = 2\left(\frac{\tau_n^m}{t_s}\right)^2 \left[\frac{t_s}{\tau_n^m} + \exp\left(-\frac{t_s}{\tau_n^m}\right) - 1\right] B_n(\bar{\sigma}, k_c) \tag{9}$$

with τ_n^m the correlation time, B'_n the experimentally measured amplitudes, B_n the corrected values, and n and m the orders of decomposition that will be introduced later. By studying 42 GUVs of egg-PC, Faucon *et al.* [70] obtained values of the k_c modulus between 0.4×10^{-19} and 0.53×10^{-19} J.

As underlined by Faucon *et al.* [70], the analysis of the thermal fluctuations of giant vesicles using video-microscopy techniques had to be limited to the first modes because of the video integration time equal to 40 ms in European standard. Using short pulses (a few ms) of light synchronized with the camera scanning allowed to get rid of this limitation [79]. A very intense light source, such as Argon laser, was thus required.

In 1992, Angelova *et al.* [33,89] made a major improvement in the precise determination of the bending elastic modulus by introducing a new protocol to form GUVs, named electroswelling or electroformation, that has been presented previously. The bending rigidities of EPC vesicles formed by this protocol were measured as a function of time, and a decrease of k_c from $(0.66 \pm 0.06) \times 10^{-19}$ J for 1 day after the vesicle formation to $(0.45 \pm 0.05) \times 10^{-19}$ J for 13 days after the vesicle formation was noticed, this last value being comparable to the bending rigidity measured for vesicles formed by gentle hydration ($(0.45 \pm 0.11) \times 10^{-19}$ J). This decrease of the bending elastic modulus was explained by the formation of lysolipids, fatty acids, and oxidation products.

In 1994, Fernandez-Puente *et al.* [71] focused their work on the effects of temperature and lipid chain length on the bending elastic modulus, which was determined following the procedure published in Refs. [70,88]. For

temperatures above the main phase transition temperature ($T_m + 6\,^{\circ}C$), the bending rigidity was found to be constant, while a strong k_c variation was noticed near the phase transition as expected theoretically [90]. A dependence on the chain length of the lipid was also observed for the bending elastic modulus (Table 11).

In 1997, Méléard *et al.* [81] studied the effect of cholesterol sulfate in DMPC bilayers with a ratio of 30 mol%, leading to an increase of k_c to $(3.8 \pm 0.2) \times 10^{-19}$ J at $T = 30\,^{\circ}C$ (Table 13). In 1998, they also focused on RBC lipids and did various measurements of the bending rigidity, for instance for some two-component lipid mixtures at room temperature [80] (Tables 5 and 16). The detailed procedure applied for these k_c determinations can be found in Refs. [70,88].

Henriksen *et al.* [91] reviewed in 2002 the treatment of the thermal undulations of quasispherical stabilized by gravity. They determined the bending rigidity in the presence of a glucose–sucrose solution system (the GUVs contained sucrose and were resuspended in equiosmolar glucose solution) and they corrected the amplitudes of fluctuations by use of the gravitational stabilization parameter, $b_n(g_0)$, found in Eq. (10), that accounted for the gravitational contribution.

$$B_n(\bar{\sigma}, k_c, g_0) = B_n^0(\bar{\sigma}, k_c)(1 + b_n(g_0)) \tag{10}$$

The purpose of using glucose and sucrose solutions was to enhance the image contrast and the yield of vesicles in the focal plane, as they were stabilized gravitationally. The effects of cholesterol, lanosterol, and ergosterol on the bending elastic modulus were measured to illustrate this new approach and the results are displayed in Table 14 [78].

In 2004, Pécréaux *et al.* [84] introduced a new method of contour analysis providing a measurement of the fluctuation spectrum of the vesicles. Improvements of both the experimental setup and the detection algorithm

Table 5 Bending rigidities obtained by studying the thermal fluctuations of GUVs at room temperature [80]

Bilayer composition (mol ratio%)	k_c ($\times 10^{-19}$ J)
SOPC	1.27 ± 0.07
SOPC[a]	1.81 ± 0.08
SOPC/gramicidin D (99.5/0.5)[a]	1.32 ± 0.06
SOPC/gramicidin D (97/3)[a]	1.38 ± 0.02
SOPC/gramicidin D (95/5)[a]	1.51 ± 0.03
EPC (1 day)	0.66 ± 0.06
DGDG	$0.08 - 0.1$

The superscript [a] indicates that the vesicles were studied in a buffer solution (pH 7.4).

allowed an analysis at higher modes than previously done. The global fluctuation spectrum was directly fitted to deduce simultaneously the membrane tension and the bending modulus of lipid membranes. Notice that this analysis was not restricted only to quasispherical vesicles, as the high modes do not depend on the shape. The vesicle fluctuation spectrum was measured for some classical lipid compositions, such as EPC, SOPC, and SOPC/Chol (molecular ratio 1/1), leading to k_c values equal to $(0.45 \pm 0.09) \times 10^{-19}$, $(1.26 \pm 0.26) \times 10^{-19}$, and $(2.96 \pm 0.33) \times 10^{-19}$ J, respectively.

In 2005, Genova *et al.* [72,73] introduced the stroboscopic illumination, that consists of pulsed light illumination of a few microseconds of length, to get a better time resolution in comparison to continuous illumination of GUVs. The use of a "corrector factor" to account for the artifact due to the finite video camera integration time, that was previously presented, was thus no more necessary.

In 2006, using the experimental procedure published in Refs. [70,88], Vitkova *et al.* [87] measured the bending rigidity of lipid bilayers (DPhPC or DLPC) with increasing concentration of alamethicin, an amphiphilic peptide produced by the fungus *Trichoderma viride*. For the peptide concentrations investigated in this work, majority of the alamethicin molecules bound parallel to the membrane surface. They observed a k_c decrease with increasing the alamethicin concentration, leading thus to a behavior similar to the ones seen by other authors for membrane containing amphiphilic additives, such as mellitin [92], ion carrier valinomycin, and Ca^{2+} ionophore A23187 [93]. For instance, a reduction of the k_c modulus by a factor 2 was observed in the presence of 1 mol% of valinomycin in DMPC bilayer [93].

In 2007, Genova *et al.* [74,75] studied the influence of different sugars (two monosaccharides: glucose and fructose; three disaccharides: maltose, sucrose, and trehalose) on the bending rigidity, which was determined as indicated in Refs. [70,88], in the concentration range up to 400 mM. They observed a decrease of the bending elastic modulus for all the sugars except maltose, which did not influence the bending rigidity.

In 2008, Bouvrais *et al.* [66] performed a study of the magainin effect on the mechanical properties of POPC bilayer, by measuring in the presence of increasing concentrations of magainin the bending elastic modulus according to the theory found in Refs. [70,88]. This work will be presented in detail in the last section of this chapter to illustrate that interesting and complex information can be extracted by biophysicists using bending rigidity measurements coupled with data modeling.

In 2010, Pavlič *et al.* [83] investigated the effect of beta 2 glycoprotein I (β2-GPI), a multifunctional apolipoprotein, on the bending elastic modulus, which was determined using the procedure published in Refs. [70,88]. They showed that the bending rigidity seemed to increase slightly in the presence of the protein β2-GPI in the aqueous environment in the range from 5.5 to 55 μg/mL, with no real dependence on the concentration.

In 2010, Henriksen *et al.* [77] investigated the effects of lysolipids on the bending rigidity of POPC bilayers, which was determined as described in Ref. [78]. They observed a large decrease in κ with increasing LPC (lysophosphatidylcholine lipids) concentrations, except at the lowest concentrations where minor increases were observed. Besides, they noticed a saturation of κ for LPC16 at high concentrations, resulting from the formation of micelles above the cmc. Finally, they underlined that the degree of perturbation caused by the individual LPC molecules was dependent on the acyl-chain length, the longest acyl-chain LPC16, that displayed the smallest acyl-chain mismatch to POPC, leading to the weakest perturbation.

In 2010, Gracià *et al.* [76] studied the effect of cholesterol on two different lipid systems. The bending elastic modulus was determined by using fast digital camera to resolve small-wavelength deformations, by having acquisition time of 1 min to get a representative number of vesicle shapes, and by performing Fourier expansion of the contour. While the addition of cholesterol did not influence the bending rigidity for DOPC bilayer, the presence from 20 to 50 mol% of cholesterol in egg sphingomyelin membrane led to a gradual κ decrease of about 30%. They also measured the bending rigidity for lipid extracts from plasma membrane of human RBC with and without transmembrane peptides and did not observe any significant differences in the κ values.

In 2010, Bouvrais *et al.* [67] focused on the impact of six different commonly used fluorescent membrane probes (LAURDAN, TR-DPPE, Rh-DPPE, DiIC18, Bodipy-PC, and NBD-PC) on the bending rigidity of dye containing POPC GUVs. They used a new data analysis procedure published in Refs. [94,95] to get a more precise determination of the bending elastic modulus based on the analysis of the full probability distributions of the configurational fluctuations, displaying Gaussian statistics. They showed that the bending rigidity of POPC membranes was only weakly affected by the incorporation of 2 mol% of fluorescence probes. As this dye concentration was much higher than what is usually used in fluorescent spectroscopy or microscopy, it could be safely assumed that, under more typical conditions, the influence of the probes themselves on membrane mechanical properties was negligible. From these measurements, it appeared that the main problem was that some dyes might photoinduce lipid peroxidation. This phenomenon was associated with an unusual scattering and an increase of the bending rigidity values. This study demonstrated that bending rigidity measurements were a very sensitive tool to monitor membrane degradation and were useful to detect potential artifacts caused by the probe.

In 2011, Pakkanen *et al.* [82] looked at the impact of triolein on POPC GUVs. κ measurements performed at 24 °C according to the procedure presented in Ref. [78] indicated a huge decrease of the bending rigidity from 1.46×10^{-19} J for pure POPC bilayers to 0.66×10^{-19} J for POPC

membrane having 5 mol% of triolein, leaving a picture of these triolein-containing membranes as being extremely soft.

In 2011, Bouvrais *et al.* [65] reported the anion specificity of sodium salts on the bending rigidity of POPC lipid bilayer, whose values, that were determined as described in Refs. [94,95], are displayed in Table 15.

2.2. Techniques That Study Responses to a Mechanical Deformation

The possibility to modulate the membrane undulations by applying external mechanical deformations has been exploited to set up new techniques to measure the bending elastic modulus. Evans, Needham, and Rawicz were the first ones to use this approach with the micropipette aspiration method, where the mechanical surface tension was used to control the area absorbed by thermal shape undulations [53,96–99]. Using this concept of responses to a mechanical deformation, the bending rigidity can also be determined through tether formation [100–105], electric field deformation [76,106], measurements of beads diffusion [107], or deformation by optical force in a confocal microscope [108–110].

2.2.1. Micropipette aspiration

The first measurement of the bending elastic modulus by pipette aspiration experiments was performed in 1983 for RBC membranes by looking at cell membrane buckling and cell folding: the k_c modulus was estimated to be 1.8×10^{-19} J [96].

Evans and Needham [97] introduced in 1987 the current way to study the mechanical properties of membranes with micropipettes. Evans [53] performed bending rigidity measurements using this technique in 1990, by aspirating a giant vesicle into a small-caliber suction pipette as illustrated in Fig. 4. The analysis of the relative change in area under aspiration pressure allowed to obtain the bending rigidity from the low-tension regime of the tension–area curve.

For that, the length of the vesicle projection inside the pipette provided a direct measurement of the projected area of the vesicle so that changes in length of the vesicle projection in the pipette represented expansions of the projected area due to reduction of surface undulations and direct dilatation of area per molecule. The membrane entropic tension τ was calculated from the suction pressure ΔP (Eq. (11)), while the areal strain α was represented by the increase in projection length ΔL, assuming a constant volume (Eq. (12)).

$$\tau = \frac{\Delta P R_p}{2\left(1 - R_p/R_v\right)} \tag{11}$$

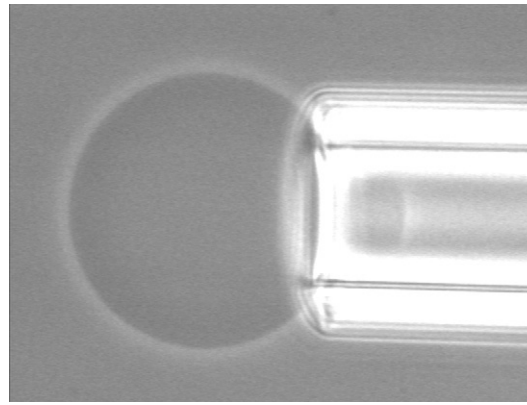

Figure 4 Aspiration of a POPC GUV with a glucose/sucrose gradient (vesicle radius: 15.9 μm and pipette radius: 7.6 μm). This image was taken by Olav Garvik from MEMPHYS lab.

Table 6 Bending rigidities obtained by micropipette aspiration of giant vesicles formed by spontaneous swelling with 0.1 M of NaCl outside and 0.1 M of sucrose inside [53]

Lipid	k_c ($\times 10^{-19}$ J)
DAPG (18 °C)	0.44 ± 0.05
DGDG (23 °C)	0.44 ± 0.03
DMPC (29 °C)	0.56 ± 0.06
SOPC (18 °C)	0.90 ± 0.06
SOPC/Chol (15 °C)	2.46 ± 0.39

$$\alpha \sim \frac{1/2\left[\left(R_p/R_v\right)^2 - \left(R_p/R_v\right)^3\right]\Delta L}{R_p} \tag{12}$$

with R_p and R_v the pipette and vesicle radii, respectively.

In the low-tension regime, the apparent expansion was dominated by smoothing of the thermal undulations and thus the elastic bending modulus was obtained from the slope of the plot of the tension logarithm versus the area dilatation ($\ln \tau$ vs. α), which was equal to $(k_B T)/(8\pi k_c)$. The first data set obtained by micropipette technique is displayed in Table 6.

Another series of measurements using the micropipette pressurization of a single vesicle was made in 2000 to study the effects of chain length and unsaturation on the bending elastic modulus [99] (Table 12).

As these measurements made by micropipette technique led to bending rigidity values lower than those obtained from shape fluctuation analysis, a paper reexamined the micropipette aspiration technique [98], where the full geometry and the full-pressure regime were taken into account, while previously approximate expressions to solve the equation of state of aspirated vesicles were applied [53,99]. By dealing with the full geometry, Henriksen and Ipsen [98] made a decomposition of the system into two subsystems: the first subsystem was constituted of a cylinder and a spherical end cap characterized by the cylinder length L and the radius R_1, respectively, and the second subsystem had a spherical-cap geometry defined by the sphere of radius R_2 and the base of R_1, as illustrated in Fig. 5. In the full-pressure regime, the relative change in area α could be approximated by Eq. (13).

$$\alpha \sim \alpha_0 + \frac{k_B T}{8\pi\kappa_{A_0}} \cdot \mathrm{In}(\sigma) + \frac{\sigma}{\nu K_a} \tag{13}$$

with α_0 a constant, κ_{A0} the bending modulus obtained assuming that the equilibrium area A_0 is constant, σ the surface tension, $\nu = A_p^{in}/A_0$ the ratio of the initial state and the equilibrium area, and K_a the area expansion modulus. The bending elastic modulus of SOPC vesicles was measured to be $(37.8 \pm 1.2)\, k_B T$ in agreement with κ values from flickering analysis found in Refs. [78,80].

2.2.2. Tether formation

The bending rigidity can be obtained through the tether formation, that is, by stretching locally the membrane to form thin cylindrical membrane strands of only 10–100 nm of diameter, called tethers. Different ways to form the tethers exist: either from phospholipid vesicles attached to micropipettes by subjecting the vesicles to the fluid drag [105] or by use of glass

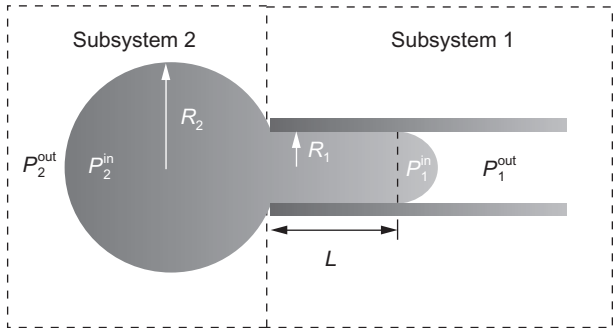

Figure 5 Illustration of the pipette geometry decomposed into two subsystems for the micropipette aspiration technique [98].

beads [100] or paramagnetic beads [102]. In the first procedure, the vesicle was held with a micropipette, which was itself positioned in the center of a much larger tube in a fluid-filled chamber, knowing that the drag force on the vesicle was controlled by adjusting the flow rate in the large tube. In the second procedure, the vesicle, on which small glass beads adhered, was aspirated into a micropipette, and the gravitational force led to the formation of a tether, by pulling it out of the surface. In the third procedure, the force on the tether was generated by an electromagnet acting on the paramagnetic bead, that was attached to the vesicle surface.

Measurements of the tether radius, R_t, as a function of the axial force on the tether, f_t, gave access to the bending stiffness, according to Eq. (14).

$$R_t = \frac{2\pi \cdot k_c}{f_t} \tag{14}$$

The tether forces were calculated either from measurements of membrane tension τ using $f_t = 2\pi R_t \tau$ [105] or from the bead radius R_b and bead density ρ_b according to the expression $f_t = 4/3\pi R_b^3 g(\rho_b - \rho_f)$ [100], with g the gravitational constant and ρ_f the fluid density. The second way presents the advantage to get an independent determination of R_t and f_t.

In 1987, Waugh *et al.* [105] measured the bending rigidity for human RBC membranes equal to 0.85×10^{-19} J. In 1989, Bo and Waugh [100] revised the paper from 1987 and showed the miss of a factor 2, which led to a new value of the bending elastic modulus of 1.7×10^{-19} J for these RBCs. They also measured the bending stiffness for SOPC vesicles and found a value of $\sim 2 \times 10^{-19}$ J for tether radii in the range of 20–100 nm.

Song and Waugh [104] used this technique to investigate the effect of cholesterol on the bending elastic modulus and measured that the curvature elastic modulus for membranes saturated with cholesterol was 3.3×10^{-19} J, about threefold larger than the modulus for cholesterol free SOPC membrane, which was in agreement with Evans observation in Ref. [53].

By varying the membrane tension of a vesicle with a micropipette and pulling a tether from this vesicle with a microsize bead manipulated with a magnetic tweezer, Heinrich and Waugh [102] determined the bending rigidity from the slope of the increase of the equilibrium tether force with the square root of the tension, giving rise to a k_c value of $(1.17 \pm 0.08) \times 10^{-19}$ J for SOPC vesicles.

In 2005, Cuvelier *et al.* [101] implemented an experimental setup based on a dual micropipette manipulation and an optical tweezer, that allowed (i) to pull two tethers from a giant vesicle, (ii) to vary the mutual distance between both vesicle-tube junctions, and (iii) to measure the force applied by one tether during the extraction. The bending rigidity and the surface tension could thus be obtained from the measurements of the angle between the two tubes and the trapping force when coalescence occurred after tube

elongation. This method offered the advantages to derive the bending stiffness with no need to control the membrane tension and to determine bending moduli for flexible membranes as well as rigid ones. This last advantage has been illustrated with the measurement of the bending rigidity of vesicles composed of BSM/Chol/mPEG-DOPE/DSPE-PEG-biotin, that were in l_o (liquid-ordered) phase, and the obtained κ value was $(66 \pm 1)\, k_B T$.

In 2010, Settles *et al.* [103] measured the contractile force f_t and the radius R_t of a tether, and this allowed them to get the modulus κ in the presence of membrane inclusions according to Eq. (15).

$$\frac{f_t R_t}{2\pi} = \kappa - \Lambda \Phi \cdot R_t \tag{15}$$

with Φ the density of inclusions and Λ a coupling constant.

They applied their technique to study the impact of Sar1, a GTPase that regulates vesicle trafficking from the ER, and observed a monotonic decrease of the bending elastic modulus as a function of Sar1 concentration, suggesting a membrane softening.

2.2.3. Deformation by electric field

In 1991, the measurement of the relative apparent dilatation of the vesicles induced by the electric field as a function of the homogeneous lateral tension allowed to obtain the bending rigidity [106]. By applying an electric field, the initial sphere was transformed into a prolate ellipsoid of revolution. The apparent increase of the membrane area with tension was due to a flattening of thermal fluctuations. The electric stresses and force densities were calculated by means of the Maxwell stress tensor and allowed to determine the lateral tension. The slope of the linear fit of the membrane area dilatation versus the logarithm of the lateral tension corresponded to the bending rigidity, as illustrated in Fig. 6. The values obtained using this technique are reported in Table 7 and appear smaller and with higher associated errors in comparison with the other techniques.

In 2010, the vesicle electrodeformation technique was used by Graciá *et al.* [76] to investigate the effect of cholesterol on DOPC bilayers and no significant change of κ was observed when varying the cholesterol amount.

Notice that this method does not apply for vesicles containing charged lipids and in the presence of salt solutions.

2.2.4. Beads diffusion

In 2000, optical dynamometry technique enabled to study the viscoelastic properties of bilayers as a function of temperature [107]. The movement of microsize latex spheres on the surface of the vesicle was thus used to provide access to several parameters. The beads could move spontaneously at the bottom of the vesicle due to the Brownian motion and could also be driven

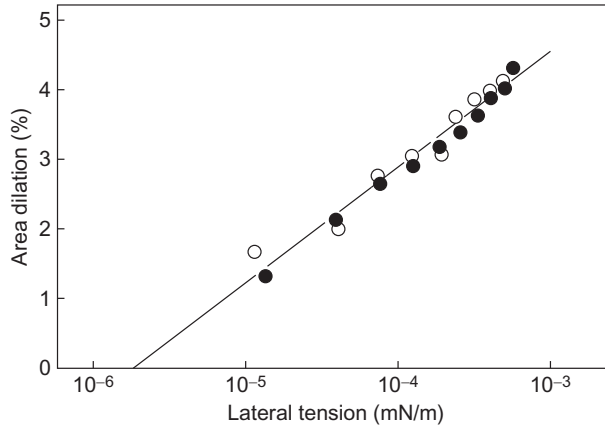

Figure 6 Apparent relative dilation of membrane area versus the logarithm of the homogeneous lateral tension [106].

Table 7 Bending rigidities of various synthetic lipids obtained by measure of giant vesicles deformation induced by electric field [106]

Lipid	k_c ($\times 10^{-20}$ J)
EYPC	2.47
DLPC	3.37
POPC	2.46
DGDG	1.01

Their errors are up to 20%.

by an external force, either the gravity sedimentation or the laser beam's radiation pressure, as shown in Fig. 7.

A static elastic experiment carried out with a double trap configuration of the laser beams allowed to obtain the elastic spring constant k_M for the gel phase, this one being related to the bending rigidity k_c according to Eq. (16).

$$k_M \sim \frac{C \cdot k_c}{R_b^2} \tag{16}$$

with C an empirical proportional constant evaluated to be equal to 60 and R_b the bead radius.

Radiation pressure forces of the laser beams were used to modify the distance between two latex particles centers, particles that had almost a point contact with the membrane. In opposition to this deformation, the membrane produced an elastic force, characterized by k_M, this

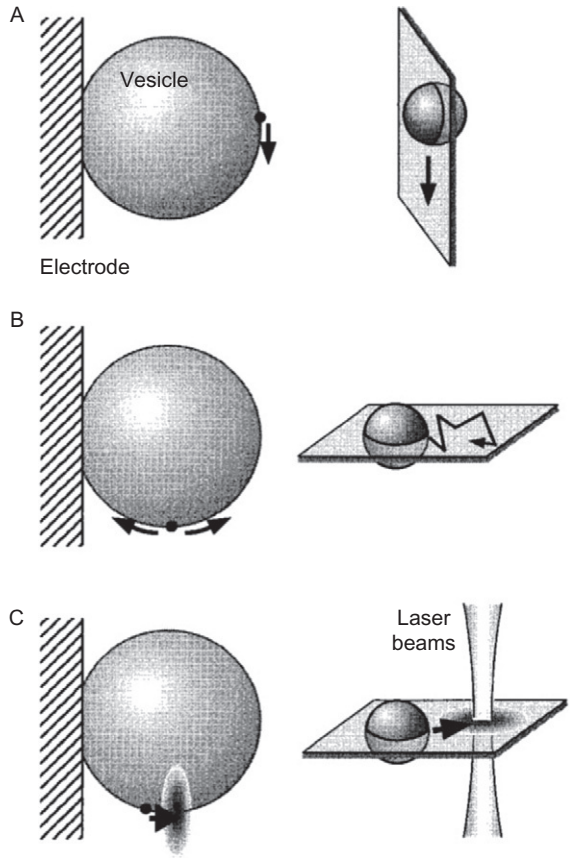

Figure 7 Schematic illustrations representing three different approaches to measure the mobility of a particle bound to the membrane: (A) gravity driven sedimentation, (B) Brownian motion at the bottom of the vesicle, and (C) optical trapping kinetics [107].

membrane response being mainly due to curvature elasticity described by the k_c modulus.

Thermal behavior of the gel-state membrane curvature modulus for DMPC vesicles was investigated with this approach allowing a direct measurement of the bending modulus of a lipid bilayer in the gel phase, as shown in Fig. 20.

2.2.5. Deformation by optical force using confocal microscopy

Confocal microscopy can also be used to give access to k_c modulus. Bending rigidity was thus studied by pressing the vesicle noninvasively with optical force and measuring its deformation directly with a nanometer-resolution

optical technique, namely, the differential confocal technique [108–110]. When the membrane, that was illuminated with a tightly focused low-power laser beam, was placed slightly above or below the focal plane, the size and divergence of the reflected beam changed sensitively with the distance between the membrane and the focal plane. The position of the membrane could be precisely determined by refocusing the retro-reflected beam at a pin-hole spatial filter and by measuring the transmitted power. The bending modulus was thus directly calculated according to Eq. (17).

$$k_c = \frac{2W}{\int_\Gamma (c_{d1} + c_{d2})^2 \mathrm{d}A - 16\pi} \tag{17}$$

with W the work done by the optical force, Γ the vesicle surface, and c_{d1}, c_{d2} the principal curvatures of an oblate spheroid.

They checked the validity of their technique by measuring the bending modulus in the fluid phase at two distinct temperatures for DMPC vesicles (Table 8) and compared the results with values obtained by the VFA in Ref. [81].

Furthermore, the bending rigidity was measured continuously across the main phase transition for DPPC vesicles, as shown in Fig. 21. These measurements were made over 30 DPPC vesicles with a k_c variation of $\pm 8.5\%$ [109]. This experiment underlines the great advantage of this technique, namely, the possibility to measure the bending rigidity in both fluid and gel phases.

2.3. Scattering Techniques

Scattering techniques are the third category of experimental techniques that can be used to obtain bending rigidity values [112–123].

First, X-ray diffuse scattering measurements can be performed on highly oriented lipid bilayers to gain access to the mechanical coefficients of bulk lamellar phases. These oriented stacks were typically in fully hydrated conditions and with spacing repeat distance d quite small so that the systems were in soft confinement regime. Both the bending elastic modulus, k_c, and

Table 8 Bending rigidities for DMPC vesicles measured by optical force in a confocal microscope prepared by the procedure of Akashi *et al.* [17] (lipid film hydration) with 0.1 M of sucrose inside and 0.1 M of glucose outside [109]

Temperature (°C)	k_c ($\times 10^{-19}$ J)
27	1.41 ± 0.13
30	1.33 ± 0.12

the interaction modulus, B, could be extracted and were related to the Caillé parameter, η_c, and the in-plan correlation length, ξ, is obtained from the scattering data according to Eq. (18) [118].

$$\eta_c = \frac{k_B T}{8\sqrt{B k_c}} \cdot \frac{4\pi}{d^2} \quad \text{and} \quad \xi^4 = \frac{k_c}{B} \tag{18}$$

Caillé theory [124] accounts for the elastic deformations of the layer positions, where the free energy density $\mathcal{G}$ is defined by Eq. (19).

$$\mathcal{G} = \frac{k_c}{2}\left(\frac{\partial^2 u}{\partial x^2} + \frac{\partial^2 u}{\partial y^2}\right)^2 + \frac{B}{2}\left(\frac{\partial u}{\partial z}\right)^2 \tag{19}$$

with $u(x,y,z)$ the local displacement of the layers along the z direction normal to the layers.

The Caillé parameter and the in-plan correlation length can be obtained thanks to the analysis of the tails of the diffraction peaks and the intensity in the very small angle regime ($q_z < 0.03$ Å), respectively. However, in practice the in-plan correlation length ξ could not be obtained as described above because the intensity in this region was too weak and could be obscured by the black beam so that the parameters η_c and ξ were obtained from the q_r dependence of the data at large q_z values. The fluctuations and diffuse scattering were dominating in large regions of these data so that the important unknowns were the two parameters η_c and ξ and the form factor $F(q_z)$. As the factor F depended only on q_z, both the parameters η_c and ξ could be found by focusing only on the q_r dependence and by looking at two q_z slices of data. This is illustrated in Fig. 8 for a DOPC fully hydrated L_α phase at 30 °C, where the values $\eta_c = (0.08 \pm 0.04)$ and $\xi = (59 \pm 2)$ Å were extracted from the spectrum leading to the following values for both moduli: $k_c = (0.8 \pm 0.08) \times 10^{-12}$ erg and $B = (10.3 \pm 3.09) \times 10^{12}$ erg/cm^4 [118]. In 2004, other measurements were made on the same system, namely, DOPC at 30 °C [117].

Furthermore, some measurements of the bending elastic modulus were performed at 30 °C for various lipid systems with the following results: $k_c = 6.9 \times 10^{-20}$ J for DMPC [115], $k_c = 5.5 \times 10^{-20}$ J for DLPC [115], $k_c = 0.85 \times 10^{-19}$ J for POPC [116], and $k_c = 1.27 \times 10^{-19}$ J for di22:1-PC [116].

Temperature effect on the bending rigidity was also investigated by this technique and a decrease of the k_c modulus was observed when the temperature approached the phase transition temperature (Fig. 22), which was shown to correlate with the anomalous swelling of lipid bilayer stacks [114]. The salt effect for DLPC bilayers [121] and the temperature dependence of DOPC bilayers [126] (Fig. 23) on the bending rigidity were also studied using this scattering technique.

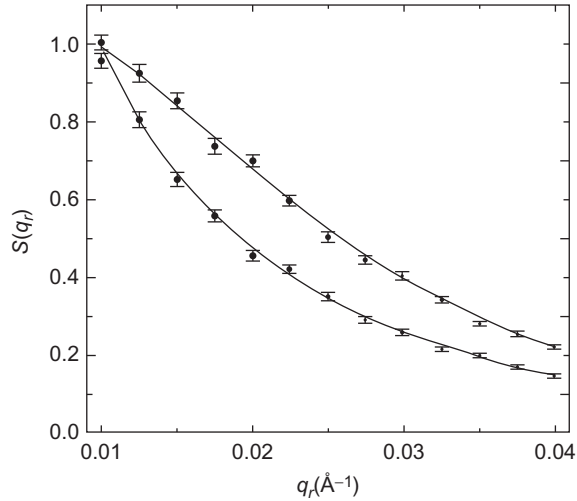

Figure 8 A nonlinear least-squares fit to two slices of data producing the two solid curves and returning the values of η_c and ξ [118].

Besides, by measuring the bending rigidity for four kinds of lipids (DMPC, SOPC, DOPC, and diC22:1-PC) in the presence of cholesterol, it was recently shown by Pan *et al.* [119,120] that the effect of cholesterol on mechanical properties depends on the degree of lipid chain saturation (Fig. 25).

Alternatively, scattering measurements can be performed on LUVs prepared by extrusion method. The combination of Neutron Spin Echo (NSE) and Dynamic Light Scattering (DLS) enabled Arriaga *et al.* [112,113] to study the shape fluctuations of bilayer vesicles. The Zilman–Granek model [127], that defines the q^3 dependence of the relaxation rates of the shape fluctuations according to Eq. (20), was used to measure the bending modulus of the lipid bilayer.

$$\Gamma \simeq 0.025 \left(\frac{k_B T}{\kappa}\right)^{1/2} \left(\frac{k_B T}{\eta}\right) q^3 \tag{20}$$

with q the fluctuation wave vector, η the viscosity of the fluid medium, and Γ the relaxation rate of the shape fluctuations.

While the center-of-mass diffusion translation is expected to be dominant in the DLS-window, shape deformation can be considered as the main scattering contribution in the NSE data. Thus, the DLS experiments enabled to get first the values of the translational diffusion coefficient and hydrodynamic radius, which were later used to analyze the NSE scattering

functions. Finally, the relaxation frequency of the fluctuation modes was determined from the fitting of the experimental NSE relaxation functions.

Arriaga *et al.* [112] used this approach to determine the bending rigidity for POPC vesicles containing different amounts of cholesterol. The presence of cholesterol in the bilayer led to larger relaxation times and hence to smaller relaxation rates of the undulation bending modes. The resulting κ values were in the range of 19–37 k_BT depending on cholesterol content.

Finally, another experimental technique to determine the bending rigidity can also be classified in this category, combining both flickering and scattering. Zilker *et al.* [122,123] used dynamic Reflection Interference Contrast (RIC) microscopy to look at thermally excited surface undulations of membranes. The interference of light reflected from cell surface and from the cover glass, to which the cells were slightly fixed, led to the formation of a Newtonian interference pattern, which was analyzed by a homemade fast image processing system. The lower membrane of cells was attached to substrate at only a few discrete points to prevent lateral motion of the whole cell without significantly attenuating membrane fluctuations. The Fourier transformation of the RIC interference pattern allowed to determine the spatial frequency spectrum of the flickering and thus the bending elastic modulus k_c in a wave-vector regime between 0.3 and 4 μm^{-1}. Hence, RIC microscopy in combination with real-time image processing enabled precise measurements of the wave-vector dependence of membrane fluctuation amplitudes over an order of magnitude of the wave vector.

The bending elastic moduli of various erythrocytes plasma membranes were compared using this technique, leading to the values of $(3.4 \pm 0.8) \times 10^{-20}$ J for normal discocytes and cup-shaped stomatocytes, and $(13 \pm 2) \times 10^{-20}$ J for echinocytes [122]. Later, measurements were performed for discocyte cells and DMPC bilayers leading to k_c equal to $(2.3 \pm 0.5) \times 10^{-20}$ and $(4.6 \pm 1.5) \times 10^{-20}$ J, respectively [123].

2.4. Molecular Dynamics Simulations

MD simulations have moved into the mesoscopic regime in the late 1990s taking advantage of the increased computer power and advances in simulation algorithms [128]. In the mesoscopic regime, collective phenomena such as the membrane spontaneous undulations have been observed, which has led to accurate estimates of mesoscopic properties such as the bending elastic modulus we are interested in here.

The most common approach in MD simulations to obtain the bending rigidity is the "flicker spectroscopy" with coarse-grained as well as atomistic methods. This category of simulations is based on a two-step strategy: (i) study of the boundary conditions effect on the membrane behavior and determination of the lateral tension induced in the membrane by these boundary conditions so that the parameter values that correspond to

tensionless states are identified and (ii) detailed analysis of the shape fluctuations of the membrane in its tensionless state. Several independent MD simulations employing either detailed atomistic or coarse-grained models have demonstrated that the lipid bilayer thermal fluctuations followed the Helfrich model prediction, that is, that the magnitude of the thermal fluctuations of a bending mode with wave number q was proportional to q^{-4} in the long wavelength regime, namely, wavelengths that were almost as small as the membrane thickness. The first determination of a bending elastic modulus from a MD simulation was obtained by Goetz *et al.* [129] in 1999 with a coarse-grained method, and this led to a value of 7.4 k_BT for an amphiphilic molecule consisted of one lyophilic headgroup particle connected to a chain of four lyophobic particles. Later, numerous coarse-grained simulations have been performed and provided, for instance, values of the bending modulus for DMPC [130] and DPPC [131,132]. Furthermore, some coarse-grained simulations were even able to show the correct κ dependence on both the temperature [133] and the hydrophobic length of the tails [133,134]. Several coarse-grained simulations have also been able to catch the correct order of magnitude of the bending rigidity for amphiphilic molecules composed of either a single hydrophobic tail [129,134,135] or two hydrophobic tails [130–133,136–138]. A few atomistic simulations have additionally been used to look at membrane undulations but to a smaller extent, as these simulations, that have the advantage to represent explicitly the chemistry of the lipids, are computationally demanding and thus limited to relatively small length and time scales. With such atomistic methods, bending rigidities were determined for DPPC, glycerolmonooolein, and sphingomyelin, leading to κ values equal to 5×10^{-20} J [139], $(4 \pm 2) \times 10^{-20}$ J [140], and $(41.2 \pm 1.9) \times 10^{-20}$ J [141], respectively.

Very few simulations are based on the other general approach typically used experimentally to determine the bending rigidity, namely, the measurement of the force needed to actively bend the membrane. While den Otter and Briels [142] introduced a method, where constraining forces were applied to actively deform the membrane, Farago and Pincus [143] presented a method based on the change in free energy of deforming the bilayer. In fact, σ and κ described the free energy variations due to area-changing and curvature-forming deformations and therefore could be related to the derivatives of the partition function with respect to the relevant strain variables. This approach, namely, an "active method," is not commonly used because of the technical and conceptual sophistication, even if it may be an interesting alternative to study the stiff membranes, as the thermally excited amplitudes are smaller in this case and thus difficult to resolve.

An alternative approach proposed by Harmandaris and Deserno [144] consisted in measuring the force necessary to hold a membrane tether and was thus conceptually identical to its experimental "counterpart." The basic idea was to create a curved cylindrical vesicle and then measure the force

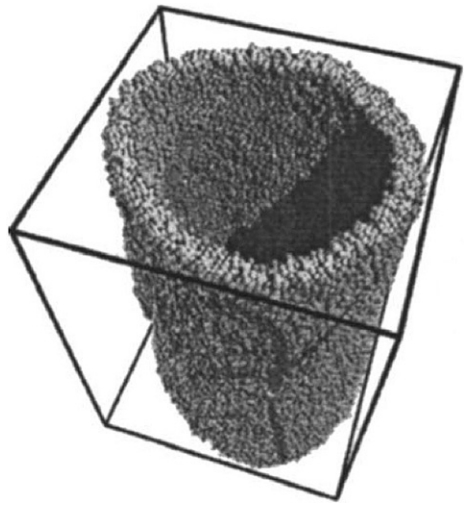

Figure 9 Snapshot of a tether simulation with 20,000 lipids [144].

Table 9 Bending rigidities of DOPC lipid bilayers at different fullerene concentrations obtained from tether simulations [146]

Fullerene concentration [mol%]	κ ($\times 10^{-20}$ J)
0	5.5 ± 1.0
1.4	5.1 ± 1.2
5.5	4.9 ± 0.6
11.1	4.4 ± 0.6

Results were the averages over three independent simulations.

required to hold it in this deformed state. The tether was simply created by "spanning" a cylindrical vesicle through the simulation box across the periodic boundary conditions as illustrated in Fig. 9, and it was then required to measure its equilibrium radius as well as the tensile force the tether exercised on the box. This axial pulling force was obtained from the component of the stress tensor along the box-spanning direction. Applying this simulation to a lipid composed of a hydrophilic head bead and two hydrophobic tail beads led to a κ value equal to $(11.7 \pm 0.2)\, k_B T$ [144]. This approach was used to measure the bending rigidity of a binary system DPPC/DOPG, with the ratios 4:1 and 1:1 giving rise to κ values equal to $(2.7 \pm 0.5) \times 10^{-19}$ and $(1.8 \pm 0.6) \times 10^{-19}$ J, respectively [145]. Later, the effect of fullerene in DOPC lipid bilayers was investigated by performing tether simulations to determine fullerene-induced changes in the bending rigidity and these results are displayed in Table 9 [146].

2.5. Comparison of Bending Rigidity Values for the Same System

We can notice that for one-component membranes composed of the same lipid, different values of the bending elastic modulus have been obtained depending on the techniques employed, as illustrated in Table 10 with κ values of SOPC lipid bilayers. A few explanations to these differences can be put forward: (i) the experimental conditions used are not completely identical (changes in pH or temperature, differences in the composition of the buffer solution, purity of lipids, aging of vesicles, etc.) and we illustrate in the last section that such "environmental conditions" may matter as the bending rigidity can depend, for instance, on the salt composition and concentration, (ii) some area excess could be hidden in membrane [150], and (iii) the length scales investigated might be different among the techniques (e.g., only the short wavelength regime is captured by the flickering technique).

3. Focus on the Flickering Technique of GUVs

As read in the previous section, many measurements of the bending rigidity have been obtained using the flickering technique of GUVs, explaining why an entire section of this chapter is dedicated to the theoretical and experimental procedures involved in this technique. The state of art of the theory behind the flickering technique of GUVs presented in this

Table 10 Bending rigidities for SOPC bilayers obtained from various techniques

Technique	κ ($\times 10^{-19}$ J)
Micropipette, tether formation [100]	2.0
Micropipette aspiration [53]	0.90 ± 0.06
Micropipette, tether formation [104]	~ 1.2
Micropipette, tether formation [102]	1.17 ± 0.08
Flickering of quasispherical vesicles [93]	1.44 ± 0.35
Flickering of quasispherical vesicles [80]	1.27 ± 0.07 (pH 5.5)
Flickering of quasispherical vesicles [80]	1.81 ± 0.08 (pH 7.4)
Micropipette aspiration [99]	0.9 ± 0.06
Flickering of prolate vesicles [147]	1.44 ± 0.12
Micropipette aspiration [148]	0.48
Micropipette aspiration [98]	1.56 ± 0.05
Flickering of quasispherical vesicles [84]	1.26 ± 0.26
Micropipette [149]	0.48 ± 0.03

Notice that the ordering is according to year of publication.

section is mainly coming from theoretical works performed successively by Faucon *et al.* [70], Mitov *et al.* [88], and Méléard *et al* [95].

3.1. From the Theoretical Model to the Experiments

3.1.1. Parameterization and Hamiltonian

Values of the bending rigidity can be extracted from thermally induced shape undulations of the membrane. The vesicles of interest for the flickering technique are in fluid phase, unilamellar, and with a radius of several micrometers. As mentioned in Section 1, the bilayer thickness is about twice the length of the lipid molecules ($\sim$50 Å). Furthermore, the membrane out of plane undulations is large compared to membrane thickness. Thus, about three orders of magnitude separate the bilayer thickness and the size of a vesicle visible by optical microscopy so that the membrane can be described as a fluctuating bidimensional surface in a tridimensional space (the solvent) that is, a smooth surface with $\mathrm{d}A$ a differential area element and $A = \int \mathrm{d}A$ its total area. As the membranes investigated with this experimental approach are fluid, the description of membrane conformations cannot depend on the molecular coordinates. The language of differential geometry with surface invariants appears thus to be appropriate for this purpose.

3.1.1.1. Parameterization of the surface In differential geometry, point positions on a bidimensional surface are specified by a tridimensional vector $\overrightarrow{R}(u)$, that is function of two coordinates $u = (u_1, u_2)$ [151]. Membranes are thus parameterized by two variables u_1 and u_2 and infinitesimal displacements along the surface satisfy Eq. (21).

$$d\overrightarrow{R} = \frac{\partial \overrightarrow{R}}{\partial u_1}\mathrm{d}u_1 + \frac{\partial \overrightarrow{R}}{\partial u_2}\mathrm{d}u_2 \tag{21}$$

The two surface tangent vectors at a bidimensional surface, namely, $\overrightarrow{t_1}$ and $\overrightarrow{t_2}$, that are defined according to Eq. (22), are used to construct the induced metrical tensor g_{ij} defined by Eq. (23). The metric tensor characterizes the intrinsic geometry of the surface and is used to measure infinitesimal distances between two points on the surface, while all the local properties of the surface can be expressed using the tangent vectors.

$$\overrightarrow{t_k} = \frac{\partial \overrightarrow{R}}{\partial u_k} \quad \text{for } k = \{1,2\} \tag{22}$$

$$g_{ij} = \overrightarrow{t_i} \cdot \overrightarrow{t_j} \tag{23}$$

The determinant of the metrical tensor ($g = \det(g_{ij})$) gives access to the differential area element $\mathrm{d}A$ through the definition from Eq. (24). Notice that the differential area element is an invariant under reparameterization of $\overrightarrow{R}$.

$$dA = |\overrightarrow{t_1} \times \overrightarrow{t_2}| \mathrm{d}u_1 \mathrm{d}u_2 = \sqrt{g} \mathrm{d}u_1 \mathrm{d}u_2 \tag{24}$$

The unit normal vector to the local surface $\overrightarrow{n}$ can also be constructed from the tangent vectors according to Eq. (25). The tangent plane is entirely defined and oriented by the normal vector $\overrightarrow{n}$ and its sign gives a distinction between the two sides of the surface (Fig. 10).

$$\overrightarrow{n} = \frac{\overrightarrow{t_1} \times \overrightarrow{t_2}}{|\overrightarrow{t_1} \times \overrightarrow{t_2}|} = \frac{\overrightarrow{t_1} \times \overrightarrow{t_2}}{\sqrt{g}} \tag{25}$$

The curvature tensor K_{ij} characterizes the shape of a surface and is defined by Eq. (26). K_{ij} is a 2×2 real symmetric matrix and can thus be diagonalized in an orthonormal basis, where the diagonal elements, that is, the eigenvalues C_1 and C_2, are named the principal curvatures of the local surface and define the extrinsic properties of the surface. The principal curvature axes are the inverse of the principal radii of curvature: $C_i = 1/R_i \quad \text{for } i \in \{1, 2\}$, giving access to the directions that either minimize or maximize the curvature as illustrated in Fig. 11.

$$K_{ij} = \overrightarrow{n} \cdot \partial_i \partial_j \overrightarrow{R} \tag{26}$$

with ∂_i a short notation for $\partial / \partial u_i$.

The metric tensor g_{ij} and the curvature tensor K_{ij} define completely the surface shape and its configuration, knowing that the intrinsic and extrinsic

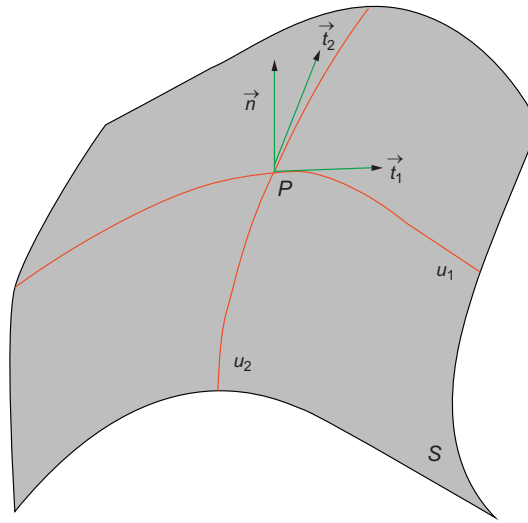

Figure 10 Differential geometry illustration: representation of a section of a surface S showing at point P the normal vector $\overrightarrow{n}$ and the tangent vectors $\overrightarrow{t_1}$ and $\overrightarrow{t_2}$.

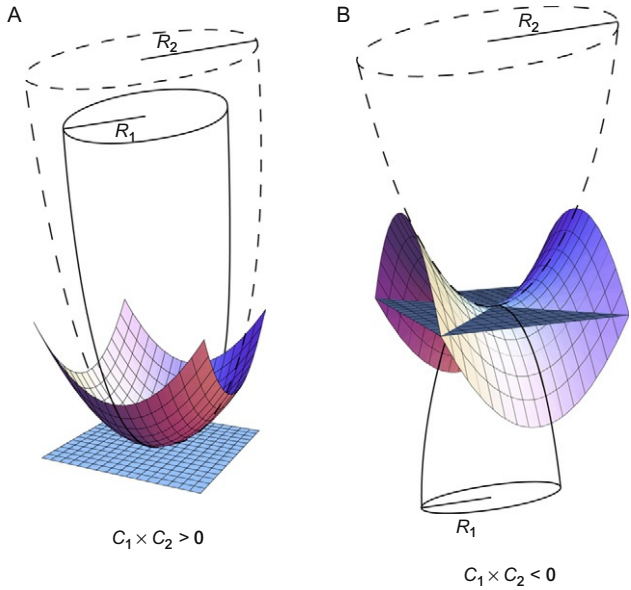

Figure 11 Radii of curvature for (A) an ellipsoidal form of the surface and (B) for a "saddle" form of the surface.

properties of the membranes are characterized by g_{ij} and K_{ij}, respectively. As the membrane is fluid, the free energy contributions describing its properties should be invariant under local changes of the surface coordinates. By combining these two tensors, two scalar surface invariants to the lowest orders in the principal curvatures respecting this constraint can be constructed: the mean curvature H (Eq. (27)) and the Gaussian curvature K (Eq. (28)).

$$H = \frac{1}{2}(C_1 + C_2) = \frac{1}{2} Tr\left(K_j^i\right) = \frac{1}{2} g^{ik} K_{kj} \tag{27}$$

$$K = C_1 \times C_2 = \det\left(K_j^i\right) = \det\left(g^{ik} K_{kj}\right) \tag{28}$$

3.1.1.2. Construction of the Hamiltonian The pioneers of the modern description of membranes and vesicle shapes are Canham [152], Helfrich [54], and Evans [153] in the early 1970s, who predicted the form of the elastic free energy by symmetry arguments and use of surface invariants introduced previously. As the amplitude of the elastic free energy depends only on the shape of the membrane, the free energy has to be an invariant with respect to a change of parameterization and can thus be described using

the both surface invariants H and K (Eqs. (27) and (28)) and the differential area element $\mathrm{d}A$ (Eq. (24)). Consequently, the free energy expression up to second order in the surface curvature radii can be constructed by additive or multiplicative combinations of the principal curvatures leading to the four following terms: $\int \mathrm{d}A$, $\int H\mathrm{d}A$, $\int H^2\mathrm{d}A$, and $\int K\mathrm{d}A$, as the mean curvature and the Gaussian curvature are in first order and in second order on the radii of curvature, respectively.

The shape of a homogeneous lipid bilayer is typically described by the phenomenological Hamiltonian for a surface, usually named the Helfrich's elastic free energy $\mathcal{H}$ (Eq. (29)), which is composed of three terms: the first term is the surface tension contribution to $\mathcal{H}$ and the second and third terms are the mean and Gaussian curvature contributions, respectively. The integrals in Eq. (29) sum all local contributions over the surface A into a single energy. Notice that this Hamiltonian has been written previously under another form in Eq. (3).

$$\mathcal{H} = \sigma \int_A \mathrm{d}A + \frac{\kappa}{2}\int_A (2H - C_0)^2 \mathrm{d}A + k_\mathrm{G}\int_A K\mathrm{d}A \tag{29}$$

The first term in Eq. (29) reflects the energy cost related to an area increase, where σ is the surface tension, that is equal to zero for a self-constituted membrane, while small surface tension is induced when a fixed volume is enclosed by the vesicle. The second term is the energy cost of bending deformation, that is, the energy cost associated with deviations of the mean curvature from a local preferred value C_0, which collects contributions from chemical and structural properties of both the membrane and the bulk, inducing spontaneous bending of the membrane. The third term measures the energy related to topology changes of the surface, where k_G reflects the cost of imposing Gaussian curvature on the surface.

In the flickering experiments, the first term in Eq. (29) is negligible and the third term in Eq. (29) is omitted (see Gauss–Bonnet theorem, Eq. (4)). Therefore, the relevant elastic free energy F_c can simply be expressed according to Eq. (30).

$$F_\mathrm{c} = \frac{\kappa}{2}\int_A (2H - C_0)^2 \mathrm{d}A \tag{30}$$

3.1.2. Quasispherical representation

Any analysis of quasispherical vesicle fluctuations starts with the identification and characterization of the vesicle contour in the focal plane. The statistical fluctuations of the contour reflect the Brownian shape fluctuations of the whole quasispherical vesicle. As the vesicles are quasispherical, that is,

surfaces in tridimensional space with nearly spherical symmetry, the polar angles (θ, ϕ) are the natural and appropriate choice for the parameterization.

The positional vector of the membrane $\overrightarrow{r}(\theta,\phi,t) = R[1+u(\theta,\phi,t)]\overrightarrow{e_r}(\theta,\phi)$ indicates the displacement of a given point of the membrane in space and with time, as illustrated in Fig. 12. The membrane configuration is represented by a displacement-field $u(\theta, \phi, t)$, which measures the local deviation from a spherical reference surface, that is, the relative amplitudes of fluctuations in the direction (θ, ϕ) and at the time t. R is the radius of the chosen reference vesicle and $\overrightarrow{e_r}(\theta,\phi)$ is the normal vector of the unit sphere. A popular choice for R is the equivalent volume sphere radius $R_v = (3V/4\pi)^{1/3}$, namely, the radius for a vesicle with the same volume than the one studied. As the fluctuations of the membrane are time-dependent thermal agitations around the equilibrium vesicle form, the vesicle shape at a given moment, $u(\theta, \phi, t)$, can be decomposed into two contributions according to Eq. (31): a static part, $u_0(\theta, \phi)$, which is the average vesicle shape, and a dynamic part of perturbation, $\delta u(\theta, \phi, t)$, giving the deviation from this equilibrium and describing the fluctuations of the vesicle, as explained in Eq. (32).

$$u(\theta,\phi,t) = u_0(\theta,\phi) + \delta u(\theta,\phi,t) \tag{31}$$

$$\langle u(\theta,\phi,t)\rangle = u_0(\theta,\phi) \Rightarrow \langle \delta u(\theta,\phi,t)\rangle = 0 \tag{32}$$

The relative membrane undulations are assumed to be small, namely, $u(\theta, \phi, t) \ll 1$, so that all the calculations are developed in the Taylor expansion up to second order in $u(\theta, \phi)$ in order to simplify the theoretical expressions.

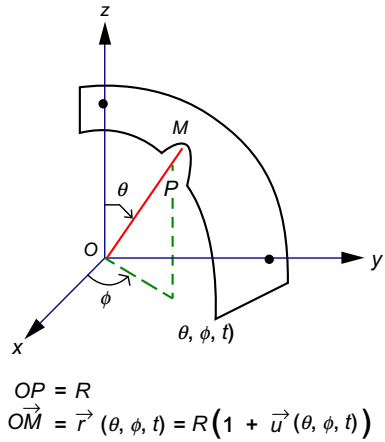

Figure 12 Sketch of the local radius deformation of a membrane with identification of the polar angles (θ, ϕ) and definition of the positional vector of the membrane $\overrightarrow{r}(\theta,\phi,t)$.

The volume of the whole vesicle, $\mathcal{V}\{u\}$ (Eq. (33)), is obtained via an integration of a volume density, $V(u)$, over all the angles ($0 \leq \theta \leq \pi$, $0 \leq \phi \leq 2\pi$). The vesicles being poorly permeable to water and salts, the exchange of water through the vesicle bilayer can be neglected. Besides, the water is an incompressible fluid. So, it can be considered that the vesicle volume does not change during the fluctuations and is thus noted as a constant $\mathcal{V}_0$.

$$\begin{aligned}\mathcal{V}\{u\} &= \oint V(u)\mathrm{d}\theta\mathrm{d}\phi = \oint R^3\left(\frac{1}{3}+u+u^2\right)\sin\theta\mathrm{d}\theta\mathrm{d}\phi \\ &= \mathcal{V}_0 = \frac{4\pi}{3}R^3\end{aligned} \tag{33}$$

The area of the whole vesicle, $\mathcal{S}\{u\}$ (Eq. (34)), is obtained via an integration of an area density function, $S(u, u_\theta, u_\phi)$, over all the angles. Due to the large values of the expansion modulus K_a, changes of the membrane area during the fluctuations are not possible leading to a constant vesicle area $\mathcal{S}_0$.

$$\begin{aligned}\mathcal{S}\{u\} &= \oint S\left(u, u_\theta, u_\phi\right)\mathrm{d}\theta\mathrm{d}\phi = \oint R^2\left[1+2u+u^2+\frac{1}{2}(\nabla u)^2\right]\sin\theta\mathrm{d}\theta\mathrm{d}\phi \\ &= \mathcal{S}_0 = 4\pi R^2(1+s)\end{aligned} \tag{34}$$

with s the area in excess over that of a sphere of equivalent volume and $(\nabla u)^2$ the square of the gradient of an unit sphere defined by Eq. (35).

$$(\nabla u)^2 = u_\theta^2 + \frac{u_\phi^2}{\sin^2\theta} \tag{35}$$

where u_θ and u_ϕ stand for the partial derivatives of u with respect to the parameters θ and ϕ, respectively.

3.1.3. Energy considerations

The bending elastic energy of the whole vesicle, $\mathcal{F}_c\{u\}$ (Eq. (36)), is obtained once again via an integration over all the angles of an energy density function, $F_c(u, u_\theta, u_\phi, u_{\theta\theta}, u_{\phi\phi})$, defined in Eq. (30).

$$\begin{aligned}\mathcal{F}_c\{u\} &= \oint F_c\left(u, u_\theta, u_\phi, u_{\theta\theta}, u_{\phi\phi}\right)\mathrm{d}\theta\mathrm{d}\phi \\ &= \oint \frac{\kappa}{2}\left[4-4\Delta u+4u\Delta u+(\Delta u)^2+2(\nabla u)^2\right]\sin\theta\mathrm{d}\theta\mathrm{d}\phi\end{aligned} \tag{36}$$

with Δu the Laplacian of an unit sphere defined by Eq. (37).

$$\Delta u = \nabla^2 u = u_{\theta\theta} + \frac{\cos\theta}{\sin\theta} u_\theta + \frac{u_{\phi\phi}}{\sin^2\theta} \tag{37}$$

where $u_{\theta\theta}$ and $u_{\phi\phi}$ stand for the second partial derivatives of u with respect to the parameters θ and ϕ, respectively.

Thermodynamical equilibrium of a fluctuating vesicle is described as the minimum of its total elastic energy. Consequently to find the equilibrium vesicle shape, the curvature energy has to be minimized at constant volume and area. This is thus a typical variational problem with two constraints that has to be solved. The method of Lagrange multipliers provides a strategy to find the maxima and minima of such a function subject to constraints. Thus, Eq. (38) defines a new function $\mathcal{F}\{u\}$, as a linear combination of the function that has to be minimized, $\mathcal{F}_c\{u\}$, with the two constraints, $\mathcal{S}\{u\}$ and $\mathcal{V}\{u\}$. The function $\mathcal{F}\{u\}$ is analyzed later as a function being without any constraint.

$$\mathcal{F}\{u\} = \mathcal{F}_c\{u\} + \sigma\mathcal{S}\{u\} - \Delta p\mathcal{V}\{u\} \tag{38}$$

where the membrane tension σ and the difference between the internal and external hydrostatic pressures Δp are the Lagrange multipliers associated to the both constraints.

Looking for the function u_0, that minimizes the function $\mathcal{F}\{u\}$, is equivalent to solving the system of Eq. (39).

$$\begin{cases} \delta\mathcal{F}\{u_0,\delta u\} = \delta\mathcal{F}_c\{u_0,\delta u\} + \sigma\delta\mathcal{S}\{u_0,\delta u\} - \Delta p\delta\mathcal{V}\{u_0,\delta u\} = 0 \\ \delta^2\mathcal{F}\{u_0,\delta u\} = \delta^2\mathcal{F}_c\{u_0,\delta u\} + \sigma\delta^2\mathcal{S}\{u_0,\delta u\} - \Delta p\delta^2\mathcal{V}\{u_0,\delta u\} \geq 0 \end{cases} \tag{39}$$

The following expressions of $\delta\mathcal{F}_c$, $\delta\mathcal{S}$, and $\delta\mathcal{V}$ are obtained by derivation of Eqs. (36), (34), and (33), respectively (see Ref. [154] for details).

$$\delta\mathcal{F}_c = \kappa\oint([\Delta(\Delta u_0) + 2\Delta u_0]\sin\theta)\delta u \mathrm{d}\theta\mathrm{d}\phi \tag{40}$$

$$\delta\mathcal{S} = R^2\oint([2 + 2u_0 - \Delta u_0]\sin\theta)\delta u \mathrm{d}\theta\mathrm{d}\phi \tag{41}$$

$$\delta\mathcal{V} = R^3\oint([1 + 2u_0]\sin\theta)\delta u \mathrm{d}\theta\mathrm{d}\phi \tag{42}$$

Looking at the minimum of the free energy $\mathcal{F}$ enables to get the Euler–Lagrange equation, defined by Eq. (43), which is an expression that is satisfied by all functions u_0 representing an equilibrium shape of the vesicle.

$$\delta\mathcal{F} = 0 \Rightarrow \Delta(\Delta u_0) + (2 - \bar{\sigma})\Delta u_0 + 2(\bar{\sigma} - \bar{p})u_0 = \bar{p} - 2\bar{\sigma} \tag{43}$$

with $\bar{\sigma} = \sigma R^2/\kappa$ the reduced membrane tension and $\bar{p} = \Delta p R^3/\kappa$ the reduced pressure difference.

The second variation of the function $\mathcal{F}$, which is a quadratic form of the perturbations δu, can be transformed via integrations by parts in a more convenient form displayed by Eq. (44), which is the product of δu with a linear differential operator $\mathcal{L}\{u_0\}$ (see Ref. [154] for the details regarding the derivation of Eq. (44)).

$$\delta^2\mathcal{F}\{u_0,\delta u\} = \kappa \oint\!\!\!\oint \delta u[\mathcal{L}\{u_0\}]\delta u \mathrm{d}\theta \mathrm{d}\phi \tag{44}$$

where $[\mathcal{L}]\delta u = [\Delta(\Delta\cdot) + (2-\bar{\sigma})\Delta\cdot + 2(\bar{\sigma}-\bar{p})\cdot]\delta u$.

The eigenfunctions of the linear operator $\mathcal{L}$ are the well-known spherical harmonics functions $Y_n^m(\theta,\phi)$ defined by Eq. (45), which are the relevant basis for diagonalization in the spherical geometry.

$$Y_n^m(\theta,\phi) = (-1)^m \sqrt{\frac{(2n+1)(n-m)!}{4\pi(n+m)!}} P_n^m(\cos\theta)\exp(jm\phi) \tag{45}$$

where $P_n^m(\cos\theta)$ are the associated Legendre polynomials, with n and m the orders of decomposition and $j = \sqrt{-1}$.

Equation (45) can be decomposed according to Eq. (46).

$$Y_n^m(\theta,\phi) = \Theta_n^m(\theta) \times \Phi_n^m(\phi) \tag{46}$$

where

$$\begin{cases} \Phi_n^m(\theta) = (-1)^m \sqrt{\dfrac{(2n+1)(n-m)!}{2(n+m)!}} P_n^m(\cos\theta) \\ \Phi_n^m(\phi) = \dfrac{1}{\sqrt{2\pi}} \exp(jm\phi) \end{cases} \tag{47}$$

Notice that in the quasispherical approach, the Laplacian presents the nice property described by Eq. (48).

$$\Delta Y_n^m(\theta,\phi) = -n(n+1)Y_n^m(\theta,\phi) \tag{48}$$

The average vesicle shape, $u_0(\theta,\ \phi)$, and the shape perturbations on the quasispherical vesicles, δu, are typically expressed in the spherical harmonics basis according to Eqs. (49) and (50), respectively.

$$u_0(\theta,\phi) = \sum_{n=0}^{n_{max}} \sum_{m=-1}^{m=n} A_n^m Y_n^m(\theta,\phi) \tag{49}$$

$$\delta u(\theta,\phi,t)=\sum_{n=0}^{n_{\max}}\sum_{m=-n}^{m=n}U_n^m(t)Y_n^m(\theta,\phi) \tag{50}$$

where A_n^m are constants; $U_n^m(t)$ the time-dependent membrane displacements in the spherical harmonics representation, as illustrated in Fig. 13; and $n_{\max}=\sqrt{N}$ an upper mode cutoff with N the number of lipid molecules constituting the vesicle membrane.

By use of the properties of the spherical harmonics, it appears that the shape perturbation functions, δu, satisfy Eq. (51) with $\lambda_n(\bar{\sigma},\bar{p})$ being the eigenvalues.

$$\mathcal{L}\{u_0\}\delta u=\lambda\delta \mathrm{u}\ =\sum_{n=0}^{n_{\max}}\lambda_n(\bar{\sigma},\bar{p})\sum_{|m|\le n}U_n^m(t)Y_n^m(\theta,\phi) \tag{51}$$

The energy function of a perturbation around the quasispherical shape can be decomposed according to Eq. (52) leading to the elastic energy cost associated to membrane fluctuations expressed in Eq. (53).

$$\mathcal{F}\{u_0,\delta u\}=\mathcal{F}\{u_0\}+\underbrace{\delta\mathcal{F}\{u_0,\delta u\}}_{=0}+\frac{1}{2}\delta^2\mathcal{F}\{u_0,\delta u\} \tag{52}$$

$$\mathcal{F}\{u_0,\delta u\}-\mathcal{F}\{u_0\}=\frac{\kappa}{2}\lambda_0(\bar{\sigma},\bar{p})|U_0^0(t)|^2+\frac{\kappa}{2}\sum_{n=2}^{n_{\max}}\lambda_n(\bar{\sigma},\bar{p})\sum_{|m|\le n}|U_n^m(t)|^2 \tag{53}$$

As the Brownian motion of the vesicle as a whole does not influence the shape fluctuations, the functions U_1^m do not depend on the time, that is, $\langle U_1^m(t)\rangle=0$, explaining why in Eq. (53) the term with $n=1$ is absent.

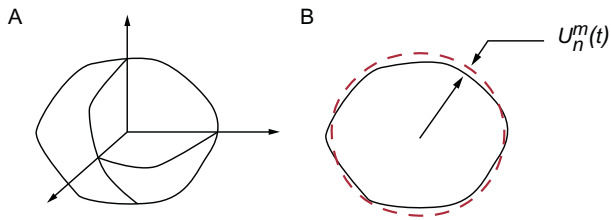

Figure 13 Schematic representation of the time-dependent membrane deformations, $U_n^m(t)$, of a vesicle in the spherical harmonics representation: (A) tridimensional view and (B) view of a horizontal cut for instance of the quasispherical vesicle. The "real" shape of the vesicle is represented by a continuous black line, while the average radius is drawn in a red dashed line.

3.1.4. Invoking the equipartition theorem

The above considerations lead to a general expression for the free energy cost of a small deviation away from the equilibrium configuration defined by Eq. (53).

Statistics are now invoked to find the probability of a deviation from the minimum energy configuration. The Boltzmann distribution for a certain deformation U_n^m is given by Eq. (54).

$$f\left(U_n^m\right) = \frac{\exp\left(-\beta\kappa/2\,\Sigma_n\lambda_n\,\Sigma_m|U_n^m|^2\right)}{\int \exp\left(-\beta\kappa/2\,\Sigma_n\lambda_n\,\Sigma_m|U_n^m|^2\right)\mathrm{d}U_n^m}, \quad n\geq 2 \text{ and } |m|\leq n \tag{54}$$

with $\beta = 1/k_\mathrm{B}T$ and $f(U_n^m)$ the frequency of getting the given amplitude of fluctuations U_n^m.

The mean square amplitude $\langle|U_n^m(t)|^2\rangle$ defined by Eq. (55) is the probable value obtained with a weight given by the Boltzmann distribution $f(U_n^m)$. $\langle|U_n^m(t)|^2\rangle$ appears to be the only contribution to the covariant matrix $\langle U_n^{m*}U_{n'}^{m'}\rangle$ according to Eq. (55).

$$\langle U_n^{m*}U_{n'}^{m'}\rangle = \int U_n^m U_{n'}^{m'} f\left(U_n^m\right)\mathrm{d}U_n^m = \delta(n,n')\delta(m,m')\langle|U_n^m(t)|^2\rangle \tag{55}$$

with $\delta(n, n')$ the Kronecker delta function.

The ergodic hypothesis allows to compute the thermal moments of U_n^m from time average over the time series. Furthermore, by invoking the equipartition theorem, that is, that each mode is contributed for an energy of $k_\mathrm{B}T/2$, the mean square values of the expansion coefficients $U_n^m(t)$ can be obtained according to Eq. (56) if the coefficients $\lambda_n(\bar{\sigma},\bar{p})$ are positive.

$$\begin{aligned} &\frac{\kappa}{2}\lambda_n(\bar{\sigma},\bar{p})\langle|U_n^m(t)|^2\rangle = \frac{k_\mathrm{B}T}{2} \\ &\Rightarrow \langle|U_n^m(t)|^2\rangle = \frac{k_\mathrm{B}T}{\kappa}\,\frac{1}{\lambda_n(\bar{\sigma},\bar{p})} \quad \text{for} \quad n\geq 2 \quad \text{and} \quad |m|\leq n \end{aligned} \tag{56}$$

For a spherical vesicle $\lambda_n = (n+2)(n-1)[\bar{\sigma}+n(n+1)]+2(2\bar{\sigma}-\bar{p})$; therefore the amplitudes of fluctuations are given by Eq. (57).

$$\langle|U_n^m(t)|^2\rangle = \frac{k_\mathrm{B}T}{\kappa}\,\frac{1}{(n+2)(n-1)[\bar{\sigma}+n(n+1)]+2(2\bar{\sigma}-\bar{p})} \tag{57}$$

As long as the fluctuations are not too large, that is, when the quadratic approximation is valid, the last term in the denominator of Eq. (57) is negligible and can therefore be omitted. This comes from the well-known

Laplace relation between the membrane tension and the transmembrane pressure difference: $\bar{p} = 2\bar{\sigma}$. Equation (57) is thus transformed in Eq. (58), expression identical to the one obtained by Milner and Safran in Ref. [155].

$$\left\langle |U_n^m(t)|^2 \right\rangle = \frac{k_B T}{\kappa} \frac{1}{(n+2)(n-1)[\bar{\sigma} + n(n+1)]} \tag{58}$$

3.1.5. Coupling the experimental data to the theoretical angular correlation function

The flickering technique enables to collect a series of contours, which are interpreted as the cross sections of the vesicle in the focal plane of the microscope, giving rise to the two-dimensional images of the vesicle (Fig. 14). To establish a connection between the three-dimensional elasticity model for the membrane surface developed previously and the measured two-dimensional contours, the angular correlation function has been introduced by Faucon *et al.* [70].

The cross-sectional radius $\rho(\phi, t)$, which is located at the position where the diameter of the vesicle is at its largest and the contrast is maximal, is defined according to Eq. (59), while Eq. (60) displays the cross-sectional angular correlation function for a given contour, $\xi(\gamma, t)$.

$$\rho(\phi, t) = \vec{r}(\pi/2, \phi, t) = R[1 + u(\pi/2, \phi, t)]\vec{e_r}(\pi/2, \phi) \tag{59}$$

$$\xi(\gamma, t) = \frac{1}{R^2}\left[\frac{1}{2\pi}\int_0^{2\pi} \rho(\phi + \gamma, t)\rho*(\phi, t)\mathrm{d}\phi - \rho^2(t)\right] \tag{60}$$

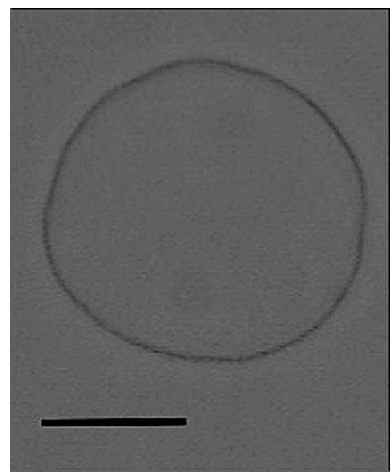

Figure 14 Image of a giant unilamellar vesicle recorded by phase contrast microscopy. The black line indicates 10 μm.

with γ the polar angle measured with respect to the horizontal axis and $\rho(t)$ the geometric average of the focal plane radius.

As seen in Eq. (59), setting the spherical coordinates $\theta = \pi/2$ gives the equatorial plane of the quasispherical vesicle, that is, the intersection of the vesicle and the focal plane of the microscope. As expressed in Eq. (61), the average focal plane radius $\rho(t)$ is obtained by integrating out from 0 to 2π the ϕ dependence in Eq. (59).

$$\rho(t) = \frac{1}{2\pi}\int_0^{2\pi} \rho(\phi, t)\mathrm{d}\phi \tag{61}$$

3.2. Analysis of the Membrane Fluctuations to Get the Bending Rigidity

Two data analysis procedures of the GUVs fluctuations exist to obtain the κ modulus, namely, the average-based approach and the statistical approach.

3.2.1. Average-based approach

The approach presented below to obtain the bending elastic modulus from measurements of the thermal fluctuations of giant vesicles is the one classically used for most of the flickering measurements of κ performed on GUVs so far [66,70–75,77–83,87,156]. This approach has been well introduced theoretically in Refs. [70,88] by Mitov and co-workers.

3.2.1.1. Expression of the angular correlation function Equation (62) displays the temporal mean of the angular correlation function, $\xi(\gamma)$, in the spherical harmonics basis.

$$\xi(\gamma) = \langle \xi(\gamma, t) \rangle = \sum_{n=2}^{n_{\max}} \sum_{m \neq 0} \left\langle |U_n^m(t)|^2 \right\rangle Y_n^m(\pi/2, \gamma) Y_n^{m*}(\pi/2, 0) \tag{62}$$

Using the addition theorem of spherical harmonics explained by Eq. (63), $\xi(\gamma)$ can be decomposed in the Legendre polynomial basis according to Eq. (64).

$$P_n(\cos\gamma) = \frac{4\pi}{2n+1} \sum_{m=-n}^{+n} Y_n^{m*}(\theta_1, \phi_1) Y_n^m(\theta_2, \phi_2) \tag{63}$$

where the angle γ satisfies the relation: $\cos\gamma = \cos\theta_1 \cos\theta_2 + \sin\theta_1 \sin\theta_2 \cos(\phi_1 - \phi_2)$.

$$\xi(\gamma) = \frac{k_B T}{4\pi\kappa}\sum_{n=2}^{n_{max}}\left(\frac{2n+1}{(n+2)(n-1)[\bar{\sigma}+n(n+1)]}\right)P_n(\cos\gamma) - \frac{k_B T}{\kappa}P_0(\cos\gamma)\sum_{n=2}^{n_{max}}\frac{\left[\Theta_n^0(\pi/2)\right]^2}{(n+2)(n-1)[\bar{\sigma}+n(n+1)]} = \langle B_0\rangle \cdot P_0(\cos\gamma) + \sum_{n=2}^{n_{max}}\langle B_n(t)\rangle \cdot P_n(\cos\gamma) \quad (64)$$

The coefficients $\langle B_n(t)\rangle$, which are defined as the averages of the amplitudes of decomposition of the angular correlation function in the Legendre polynomials basis, are related to the thermodynamical quantity $\langle|U_n^m(t)|^2\rangle$ according to Eq. (65).

$$\langle B_n(t)\rangle = \begin{cases} (2n+1)/4\pi \times \langle|U_n^m(t)|^2\rangle \text{ if } n>1 \\ -\sum_{n=2}^{n_{max}} Y_n^0(\pi/2,\phi)\,Y_n^0(\pi/2,\phi)\langle|U_n^0(t)|^2\rangle \text{ if } n=0 \end{cases} \quad (65)$$

The case $n=0$ corresponds to changes in the vesicle radius, while the situations where $n=1$ are changes in the position of the vesicle's center of mass [64]. The analysis of the thermal shape fluctuations is thus based only on modes strictly above 1.

3.2.1.2. Fitting procedure to obtain the bending rigidity By invoking Eq. (58) into Eq. (65), Eq. (66) is obtained and links theoretically the average of the amplitudes of decomposition into the Legendre basis, B_n, to the two unknown parameters κ and $\bar{\sigma}$.

$$B_n(\kappa,\bar{\sigma}) = \frac{2n+1}{4\pi}\frac{k_B T}{\kappa(n+2)(n-1)[\bar{\sigma}+n(n+1)]} \quad \text{for } n>1 \quad (66)$$

The parameters, κ and $\bar{\sigma}$, and their statistical errors are finally obtained by fitting Eq. (66) to the experimental average Legendre amplitudes obtained from Eq. (64) using a χ^2-analysis over a range of modes n selected by two main criteria: (i) the first few modes are often ignored in the analysis because of large error bars due to bad statistics, as the pictures are correlated to each other, specially for the deflated vesicles, and (ii) the higher modes, with a correlation time equivalent to the video integration time, are omitted from the analysis due to smearing of the membrane contour on these length scales.

$\langle B_n(t)\rangle$ values are arithmetic means of a very large number of experimental $B_n(t)$ data (for instance, 4000 analyzed in Ref. [66], 400 in Refs. [80,81]).

The quantity $M(\kappa,\bar{\sigma})$ defined by Eq. (67) obeys a χ^2-distribution with $(N-2)$ degrees of freedom, where N is the number of modes used for the fitting procedure and D_n the standard deviations of the mean values $\langle B_n(t)\rangle$.

$$M(\kappa,\bar{\sigma}) = \sum_{n=2}^{n=N+1} \left(\frac{B_n(\kappa,\bar{\sigma}) - \langle B_n(t)\rangle}{D_n} \right)^2 \tag{67}$$

3.2.2. Statistical approach

It is evident that many measures of the statistical contour fluctuations may provide robust means of estimating the bending rigidity κ. Such a measurement is the shape of the probability distributions of the amplitudes, which are now available due to the technical developments in data acquisition. The main contribution to $\langle |U_n^m(t)|^2 \rangle$ in the average-based approach stems from the most occupied small amplitudes of the shape fluctuations, while the information in the distribution from large amplitudes has a minor contribution as illustrated in Fig. 15. By looking at the overall distribution of the shape fluctuations, the information is extracted from a wider spectrum of amplitudes and gives more weight to the determined value of κ. This statistical approach has been presented in Refs. [94,95] and applied only for a few studies so far [65,67].

3.2.2.1. Sine and cosine transforms of the radius As stated before, studying thermal fluctuations of GUVs always starts with the determination of the position of any point of the membrane according to Eq. (68).

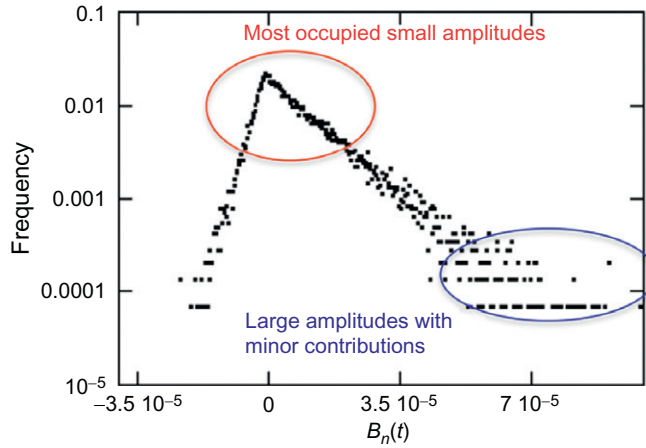

Figure 15 Experimental distribution of $B_n(t)$ for a POPC vesicle with a radius of 12.70 μm. Notice that the negative values of $B_n(t)$ observed in the distribution are "real data" and do not come from any noise contribution.

$$r(\theta,\phi,t) = R[1+u(\theta,\phi,t)]$$
$$= R\left(1+\frac{A_0^0+U_0^0(t)}{\sqrt{4\pi}}+\underbrace{\sum_{n\geq 2,|m|\leq n} U_n^m(t)\,Y_n^m(\theta,\phi)}_{=\Sigma}\right) \tag{68}$$

Equation (69) displays the spherical harmonics functions $Y_n^m(\theta,\phi)$ already introduced in Eq. (45), which are expressed here with the normalized generalized Legendre polynomials $\mathcal{P}_n^m$, themselves defined by Eq. (70).

$$Y_n^m(\theta,\phi) = \mathcal{P}_n^m(\cos\theta)\exp(jm\phi) \tag{69}$$
$$\mathcal{P}_n^m(x) = (-1)^m\sqrt{\frac{(2n+1)(n-m)!}{4\pi(n+m)!}}P_n^m(x) \tag{70}$$

Using the general relation $P_n^{-m}(x) = (-1)^m(n-m)!/(n+m)!\,P_n^m(x)$ [157], one gets $\mathcal{P}_n^{-m}(x) = (-1)^m\mathcal{P}_n^m(x)$. Consequently, the last summation in Eq. (68) can also be written according to Eq. (71).

$$\Sigma = \sum_{n\geq 2}\left[U_n^0(t)\,Y_n^0(\theta,\phi)+\sum_{0<m\leq n}\left(U_n^m(t)\,Y_n^m(\theta,\phi)+U_n^{-m}(t)\,Y_n^{-m}(\theta,\phi)\right)\right]$$
$$= \sum_{n\geq 2}\left[U_n^0(t)\,Y_n^0(\theta,\phi)\right.$$
$$\left.+\sum_{0<m\leq n}\left(\underbrace{U_n^m(t)\exp(jm\phi)+(-1)^m U_n^{-m}(t)\exp(-jm\phi)}_{\Omega_n^m}\right)\mathcal{P}_n^m(\cos\theta)\right] \tag{71}$$

Writing $U_n^m(t) = \left(a_n^m(t)-jb_n^m(t)\right)/2$ and $U_n^0(t) = a_n^0(t)$, one obtains Eq. (72) for the expression of Ω_n^m. Notice that the references to the time t have been dropped for simplification.

$$\Omega_n^m = \frac{a_n^m\cos(m\phi)+b_n^m\sin(m\phi)+(-1)^m\left[a_n^{-m}\cos(m\phi)-b_n^{-m}\sin(m\phi)\right]}{2}$$
$$+j\frac{a_n^m\sin(m\phi)-b_n^m\cos(m\phi)+(-1)^m\left[-a_n^{-m}\sin(m\phi)-b_n^{-m}\cos(m\phi)\right]}{2} \tag{72}$$

Since real functions are expected, the last part of Eq. (72) has to cancel, which leads to the two equalities defined by Eqs. (73) and (74).

$$a_n^m(t) = (-1)^m a_n^{-m}(t) \tag{73}$$

$$b_n^m(t) = -(-1)^m b_n^{-m}(t) \tag{74}$$

Consequently, Eq. (72) is transformed in Eq. (75),

$$\Omega_n^m = a_n^m \cos(m\phi) + b_n^m \sin(m\phi) \tag{75}$$

and Eq. (71) in Eq. (76).

$$\Sigma = \sum_{n\geq 2}\left[a_n^0 \mathcal{P}_n^0(\cos\theta) + \sum_{0<m\leq n}\left(a_n^m \cos(m\phi) + b_n^m \sin(m\phi)\right)\mathcal{P}_n^m(\cos\theta)\right] \tag{76}$$

Applying Eq. (76) in Eq. (68), the expression of the radius using Fourier decomposition can thus be expressed simply according to Eq. (77).

$$\begin{aligned} r(\theta,\phi,t) = R\Bigg(1 + \frac{A_0^0 + U_0^0(t)}{\sqrt{4\pi}} \\ + \sum_{n\geq 2}\left[a_n^0 \mathcal{P}_n^0(\cos\theta) + \sum_{0<m\leq n}\left(a_n^m \cos(m\phi) + b_n^m \sin(m\phi)\right)\mathcal{P}_n^m(\cos\theta)\right]\Bigg) \end{aligned} \tag{77}$$

3.2.2.2. Energy distributions The Taylor expansion of the free energy to the second order in δu has been developed in detail previously in this chapter (Eq. (53)), and it has been shown that the free energy of vesicle fluctuations is described according to Eq. (78).

$$\mathcal{F}\{u_0, \delta u\} - \mathcal{F}\{u_0\} = \frac{\kappa}{2}\lambda_0(\bar{\sigma})|U_0^0(t)|^2 + \frac{\kappa}{2}\sum_{n=2}^{n_{\max}}\lambda_n(\bar{\sigma})\sum_{0\leq|m|\leq n}|U_n^m(t)|^2 \tag{78}$$

where $\lambda_n(\bar{\sigma}) = (n+2)(n-1)[\bar{\sigma} + n(n+1)]$, after having dropped the $\bar{p}$ Lagrange multiplier in comparison to Eq. (53).

The energy expression (78) can be rearranged into Eq. (79).

$$\begin{aligned} \mathcal{F}\{u_0, \delta u\} - \mathcal{F}\{u_0\} = \frac{\kappa}{2}\lambda_0(\bar{\sigma})|U_0^0(t)|^2 \\ + \frac{\kappa}{2}\sum_{n=2}^{n_{\max}}\lambda_n(\bar{\sigma})\left(|U_n^0(t)|^2 + \sum_{1\leq|m|\leq n}\left[|U_n^m(t)|^2 + |U_n^{-m}(t)|^2\right]\right) \end{aligned} \tag{79}$$

Equations (80) and (81) are obtained by using the definitions of $a_n^m(t)$ and $b_n^m(t)$ and the expecting real values for $r(\theta, \phi, t)$ (Eqs (73) and (74)).

$$|U_n^0(t)|^2 = |a_n^0(t)|^2 \tag{80}$$

$$|U_n^m(t)|^2 + |U_n^{-m}(t)|^2 = \frac{1}{2}\left[|a_n^m(t)^2 + |b_n^m(t)|^2\right] \quad \text{with } n \geq m \geq 1 \tag{81}$$

Eliminating $|U_0^0(t)|^2$ as a fourth order term [88] and using Eqs. (80) and (81), the free energy can be expressed with the Fourier amplitudes (a_n^m and b_n^m) according to Eq. (82).

$$\mathcal{F}\{u_0, \delta u\} - \mathcal{F}\{u_0\} = \frac{\kappa}{2}\sum_{n=2}^{n_{\max}} \lambda_n(\bar{\sigma}) \left(|a_n^0(t)|^2 + \frac{1}{2}\sum_{1\leq m\leq n} \left[|a_n^m(t)|^2 + |b_n^m(t)|^2\right] \right) \tag{82}$$

Applying the equipartition theorem to the free energy of Eq. (82), the expressions for the mean square values of $a_n^0(t)$, $a_n^m(t)$, and $b_n^m(t)$ can be obtained according to Eqs. (83), (84), and (85), respectively.

$$\frac{k_B T}{2} = \frac{\kappa\lambda_n(\bar{\sigma})}{2}\left\langle |a_n^0(t)|^2 \right\rangle \tag{83}$$

$$\frac{k_B T}{2} = \frac{\kappa\lambda_n(\bar{\sigma})}{4}\left\langle |a_n^m(t)|^2 \right\rangle \tag{84}$$

$$\frac{k_B T}{2} = \frac{\kappa\lambda_n(\bar{\sigma})}{4}\left\langle |b_n^m(t)|^2 \right\rangle \tag{85}$$

for $n \geq 2$ and $1 \leq m \leq n$, where $a_n^0(t)$, $a_n^m(t)$, and $b_n^m(t)$ are Gaussian fluctuating variables.

a_n^0, a_n^m, and b_n^m are independent terms contributing to the energy of the fluctuating vesicle. Thus, their corresponding Boltzmann statistics, $\mathcal{A}_n^0(x)$, $\mathcal{A}_n^m(x)$, and $\mathcal{B}_n^m(x)$, are described by Eqs. (86) and (87), respectively.

$$\mathcal{A}_n^0(x) = \sqrt{\frac{\kappa\lambda_n(\bar{\sigma})}{2\pi k_B T}} \exp\left(-\frac{\kappa\lambda_n(\bar{\sigma})x^2}{2k_B T}\right) \tag{86}$$

$$\mathcal{A}_n^m(x) = \mathcal{B}_n^m(x) = \sqrt{\frac{\kappa\lambda_n(\bar{\sigma})}{4\pi k_B T}} \exp\left(-\frac{\kappa\lambda_n(\bar{\sigma})x^2}{4k_B T}\right) \tag{87}$$

where $n \geq 2$ and $1 \leq m \leq n$ and x stands for a_n^0, a_n^m, or b_n^m.

3.2.2.3. Fourier transform of contour fluctuations As only the fluctuations in the equatorial plane can be seen due to the experimental setup, the expressions of the contour projection into the equatorial plane $\rho(\phi, t)$ (Eq. (88)) and its average $\rho(t)$ (Eq. (89)) have to be introduced and expressed using the Fourier amplitudes.

$$\rho(\phi,t) = R\left(1+\frac{A_0^0+U_0^0(t)}{\sqrt{4\pi}} + \sum_{n\geq 2}\left[a_n^0\mathcal{P}_n^0(0) + \sum_{0<m\leq n}\left(a_n^m\cos(m\phi)+b_n^m\sin(m\phi)\right)\mathcal{P}_n^m(0)\right]\right) \tag{88}$$

$$\rho(t) = \frac{1}{2\pi}\int_{\phi=0}^{2\pi}\rho(\phi,t)\mathrm{d}\phi = R\left[1+\frac{A_0^0+U_0^0(t)}{\sqrt{4\pi}}+\sum_{n=2}^{n_{\max}}a_n^0(t)\mathcal{P}_n^0(0)\right] \tag{89}$$

Thus, from Eqs. (88) and (89), one gets after some derivations Eq. (90), where the variables α^m and β^m are introduced.

$$\begin{aligned}\rho(\phi,t)-\rho(t) &= R\sum_{n=2}^{n_{\max}}\sum_{0<m\leq n}\mathcal{P}_n^m(0)\left[a_n^m(t)\cos(m\phi)+b_n^m(t)\sin(m\phi)\right]\\ &= R\sum_{0<m}^{n_{\max}}\left[\cos(m\phi)\sum_{n\geq m}^{n_{\max}}\left(a_n^m(t)\mathcal{P}_n^m(0)\right)+\sin(m\phi)\sum_{n\geq m}^{n_{\max}}\left(b_n^m(t)\mathcal{P}_n^m(0)\right)\right]\\ &= R\sum_{0<m}^{n_{\max}}\alpha^m(t)\cos(m\phi)+\beta^m(t)\sin(m\phi)\end{aligned} \tag{90}$$

Consequently, the variables $\alpha^m(t)$ and $\beta^m(t)$ are defined according to Eqs. (91) and (92), respectively.

$$\alpha^m(t) = \sum_{n\geq m}^{n_{\max}}a_n^m(t)\mathcal{P}_n^m(0) \tag{91}$$

$$\beta^m(t) = \sum_{n\geq m}^{n_{\max}}b_n^m(t)\mathcal{P}_n^m(0) \tag{92}$$

The variable α^m (resp. β^m) is a linear combination of a large number of independent fluctuating modes with Boltzmann type statistics a_n^m (resp. b_n^m) multiplied by $\mathcal{P}_n^m(0)$ as defined in Eq. (91) (resp. Eq. (92)). Knowing that the distributions (i) of a sum of random Gaussian variables and (ii) of a random Gaussian variable multiplied by a constant are both Gaussian

distributions, the variables $\alpha^m(t)$ and $\beta^m(t)$ appear to be also random Gaussian distributed, as illustrated in Fig. 16, with the experimental distributions of α^8 or β^8. Thus, the distribution of α^m (resp. β^m) called $\mathcal{A}^m$ (resp. $\mathcal{B}^m$) can simply be expressed according to Eq. (93).

$$\mathcal{A}^m(\gamma) = \mathcal{B}^m(\gamma) = \sqrt{\frac{\kappa}{4\pi k_B T \sum_{n\geq m}\left[\mathcal{P}_n^m(0)\right]^2/\lambda_n(\bar{\sigma})}} \times \exp\left[-\frac{\kappa}{4k_B T} \times \frac{\gamma^2}{\sum_{n\geq m}\left[\mathcal{P}_n^m(0)\right]^2/\lambda_n(\bar{\sigma})}\right] \tag{93}$$

where $\lambda_n(\bar{\sigma}) = (n+2)(n-1)[\bar{\sigma} + n(n+1)]$, the proportionality factor being obtained by normalization of the distribution, and γ stands for α^m or β^m.

3.2.2.4. Expression of the angular correlation function The autocorrelation function of the vesicle contour fluctuations, $\xi(\gamma, t)$, has to be introduced once again here to access a measurement of the bending rigidity, κ, and of the reduced tension, $\bar{\sigma}$. Using the angular correlation function defined by Eq. (60) and the above introduced α^m and β^m expressions, that is, Eqs. (91) and (92), one gets Eq. (94).

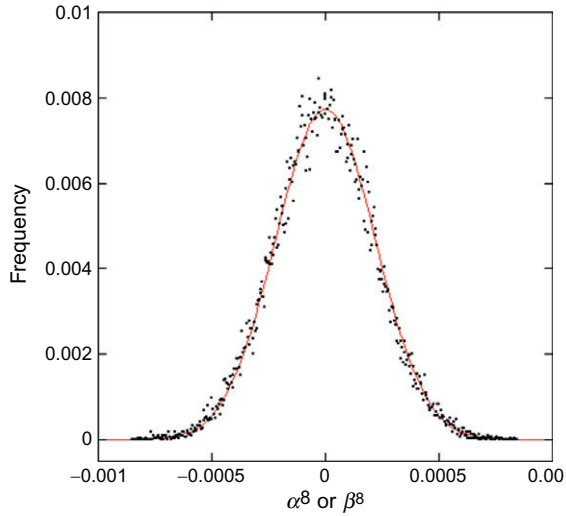

Figure 16 Experimental distribution of $\alpha^8(t)$ or $\beta^8(t)$ for a POPC vesicle with a radius of 12.70 μm (close dots) and the Gaussian fit (red full line).

$$\xi(\gamma,t)=\frac{1}{2\pi R^2}\int_{\phi=0}^{2\pi}[\rho(\phi+\gamma,t)-\rho(t)]\times[\rho(\phi,t)-\rho(t)]\mathrm{d}\phi$$

$$=\frac{1}{2\pi}\sum_{0<m}^{n_{\max}}\sum_{0<m'}^{n_{\max}}\int_{\phi=0}^{2\pi}\Big[\alpha^m(t)\alpha^{m'}(t)\cos(m\phi+m\gamma)\cos(m'\phi)$$
$$+\alpha^m(t)\beta^{m'}(t)\cos(m\phi+m\gamma)\sin(m'\phi)+\beta^m(t)\alpha^{m'}(t)\sin(m\phi+m\gamma)\cos(m'\phi)$$
$$+\beta^m(t)\beta^{m'}(t)\sin(m\phi)+m\gamma)\sin\Big(m'\phi\Big)\Big]\mathrm{d}\phi \qquad (94)$$

After some derivations, Eq. (94) defining the angular correlation function is transformed in Eq. (95).

$$\xi(\gamma,t)=\frac{1}{2}\sum_{0<m}^{n_{\max}}\left([\alpha^m(t)]^2+[\beta^m(t)]^2\right)\cos(m\gamma)=\sum_{0<m}^{n_{\max}}\xi^m(t)\cos(m\gamma) \qquad (95)$$

with the new coefficient $\xi^m(t)=\frac{1}{2}\left([\alpha^m(t)]^2+[\beta^m(t)]^2\right)$, which is defined as half a sum of two positive terms $[\alpha^m(t)]^2$ and $[\beta^m(t)]^2$, which are mono-exponential random variables.

Thus, a Fourier analysis of the autocorrelation function gives a series of ξ^m values, with typically $2\leq m\leq 20$. For a given mode m, N different values of ξ^m are obtained as a function of the recorded time t. A direct frequency representation is shown in Fig. 17, where the N obtained ξ^m values are sorted in increasing order, the smaller ξ^m close to 0 being most probable while the larger ξ^m being unlikely.

The theoretical distribution of ξ^m, called $\mathcal{G}^m$, is expected to be mono-exponential, since ξ^m is derived from the random variables α^m and β^m, which are both distributed according to Gaussian statistics $\mathcal{A}^m$ and $\mathcal{B}^m$. Equation (96) displays the full expression of the distribution of ξ^m, $\mathcal{G}^m(\xi^m)$. As shown in the inset in Fig. 17, the experimental distribution of the 8th mode as a function of the measured time-dependent amplitudes ξ^8 follows nicely the theoretically expected monoexponential behavior.

$$\mathcal{G}^m(\xi^m)=\frac{\kappa}{2k_{\mathrm{B}}T}\times\frac{1}{\sum_{n\geq m}\left[\mathcal{P}_n^m(0)\right]^2/\lambda_n(\bar{\sigma})}$$
$$\times\exp\left[-\frac{\kappa}{2k_{\mathrm{B}}T}\times\frac{\xi^m}{\sum_{n\geq m}\left[\mathcal{P}_n^m(0)\right]^2/\lambda_n(\bar{\sigma})}\right]$$

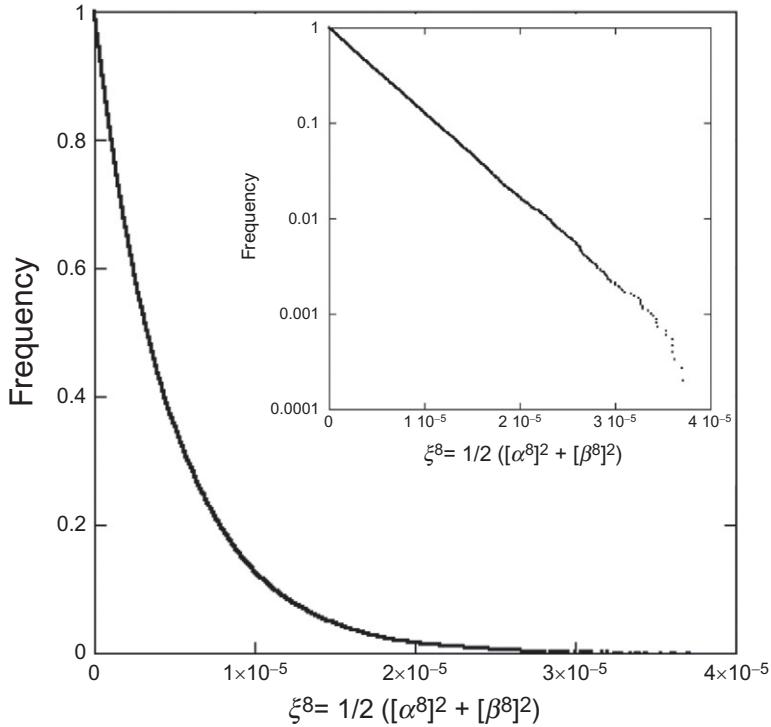

Figure 17 Experimental distribution of $\xi^8(t) = \frac{1}{2}\left(\left[\alpha^8(t)\right]^2 + \left[\beta^8(t)\right]^2\right)$ for a POPC vesicle with a radius of 12.70 μm. The same data using a semilog representation are shown in inset.

$$= \Delta^m \times \exp(-\Delta^m \xi^m) \tag{96}$$

where

$$\Delta^m = \frac{\kappa}{2k_B T} \times \frac{1}{\sum_{n \geq m} \left[\mathcal{P}_n^m(0)\right]^2 / \lambda_n(\bar{\sigma})} \tag{97}$$

with $\lambda_n = (n+2)(n-1)[\bar{\sigma} + n(n+1)]$ as mentioned previously.

3.2.2.5. Fitting procedure to obtain the bending rigidity The monoexponential behavior of the cosine decomposition of the angular correlation function appears to be followed, as observed in Fig. 18A with the distribution of the mode 8, $\mathcal{G}^8$, as a function of ξ^8, which confirms that the thermal fluctuations of the GUVs can be nicely described by this theory. However, sometimes some deviations can be noticed for the largest and uncommon amplitudes (the ones at the far right in the Fig. 18A), since they are rare events with poor statistics, and for amplitudes close to 0, as they are

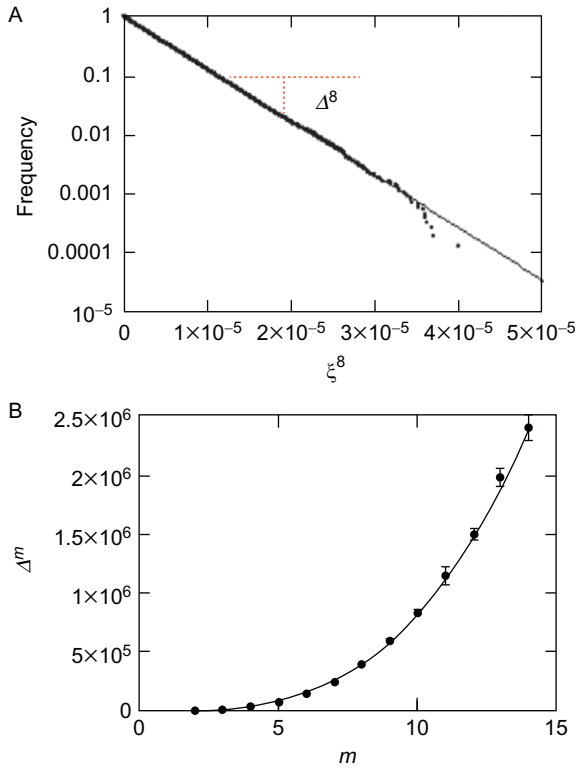

Figure 18 Experimental behavior of a 12.7-μm GUV of POPC as obtained by Fourier transform of the autocorrelation function. (A) Statistical distribution of the 8th mode (close dots) and the monoexponential fit (full line). (B) Dependence of Δ^m as a function of the mode m (close dots) up to the 14th mode and the resulting fit (full line) giving $\kappa = (31.9 \pm 0.4)\, k_B T$ and $\bar{\sigma} = (-2.9 \pm 0.6)$.

comparable to the optical resolution and thus noisy. Therefore, the decay observed in Fig. 18A is fitted using a monoexponential (Eq. (96)) with exclusion of these "outlier amplitudes" mentioned previously, namely, keeping only the frequencies between 0.4 and 0.08. These fits of the different distributions $\mathcal{G}^m$ lead to estimates of Δ^m for each mode m, as illustrated with the 8th mode in Fig. 18A.

The error on Δ^m, that is, $\sigma_\Delta{}^m$, is calculated using the discrepancy between the obtained fitted parameters when considering $0.08 \leq \mathcal{G}^m \leq 0.4$ and the full data range, namely, the square root of the sum of the squares of the linearized distribution residuals, $\sqrt{\sum_j \left(\ln\left[\mathcal{G}^m\left(\xi_j^m\right)\right] - a + \Delta^m \times \xi_j^m \right)^2}$. A true monoexponential behavior leads to very small residuals on the whole data range, and therefore a low error estimation of the experimentally

determined Δ^m is obtained from the exponential distribution of ξ^m. The discrepancy between the fitted curve and the experimental data is thus used to rank the quality of the fitted exponentials as a function of the order m.

Therefore, the values of Δ^m_{exp} and $\sigma_{\Delta^m_{\text{exp}}}$ can be obtained experimentally by analysis of the amplitude statistics of the Fourier decomposition of the autocorrelation function. As indicated in Eq. (97), Δ^m depends on the two unknown parameters, κ and $\bar{\sigma}$, and later a minimization of the merit function defined by Eq. (98) enables consequently to get particular values of both the bending rigidity and the reduced membrane tension for each vesicle, as illustrated in Fig. 18B.

$$M(\kappa,\bar{\sigma}) = \sum_{n_{\min}}^{n_{\max}} \left[\frac{\Delta^m_{\text{exp}} - \Delta^m_{\text{th}}}{\sigma_{\Delta^m_{\text{exp}}}} \right] \tag{98}$$

where $n_{\min}$ and $n_{\max}$ are, respectively, the first and last relevant modes to consider in the fitting procedure, and Δ^m_{th} the theoretical value obtained from Eq. (97).

3.2.3. Comparison between the two approaches

Figure 19 shows how well defined the bending rigidity of a one-component system can be when the statistical approach is applied. The bending rigidity averages obtained from eight POPC vesicles using either the average-based

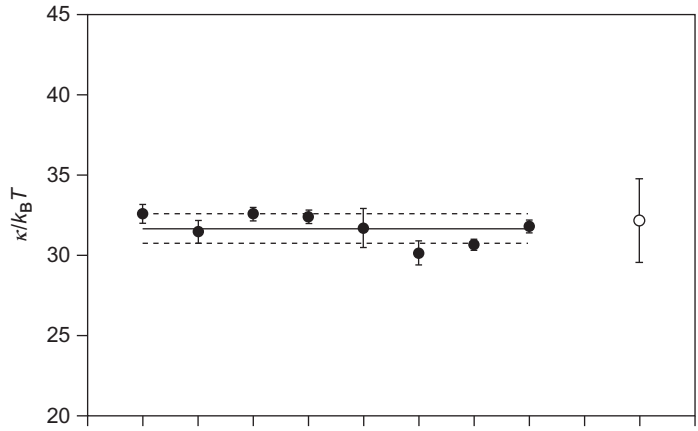

Figure 19 Comparison of the bending rigidity measurements (in k_BT units) obtained with the same eight POPC GUVs in an aqueous buffer of 1 mM Tris and 1 mM EDTA at pH 7.4. Using the average-based approach presented in Ref. [70] gives $\kappa = (32.2 \pm 2.6)\, k_BT$ (open dot), while the use of fluctuation statistics presented in Ref. [95] gives $\kappa = (31.7 \pm 0.9)\, k_BT$. For the statistical approach, each κ result is indicated by a close dot, and the full line and dotted lines are located at the average and the error width limits, respectively.

approach or the statistical one are very close, 32.2 and 31.7 k_BT, respectively. The improvement between the two approaches is visible on the standard deviation of the distribution of κ values, this one being smaller and equal to 0.9 k_BT using the statistical approach, while with the average-based one a value of 2.6 k_BT is found.

Thus, the determination of the bending rigidity using the statistical approach takes advantage of getting information from the full distributions of the amplitudes, while for the average-based approach, the κ values are simply extracted from the mean values of the amplitudes of decomposition. Besides, the new data analysis introduced with the statistical approach allows to judge GUVs behaviors by their coherence with the theoretical description of thermal fluctuations of quasispherical vesicles, namely, a monoexponential behavior of the distribution of the amplitudes of the autocorrelation function in the cosine basis, and therefore to have objective criteria to reject some vesicles for the κ determination.

4. Main Inputs from the Measurements of the Bending Rigidities

Bending rigidity measurements have given precious and interesting information to understand the lipid bilayer organization according to temperature or lipid changes, or the nature of the interactions between lipid bilayers and additive molecules.

4.1. Temperature Effect

The effect of temperature on the bending rigidity values has been studied through several works using different techniques so that both the gel and fluid phases have been investigated. The same overall behavior has been observed for DMPC and DPPC bilayers [71,81,107,109], namely, a sharp drop of the bending rigidity in the gel phase for temperature close to the main phase transition temperature T_m and a large increase of the bending rigidity in the fluid phase after the phase transition, followed by a small decrease between T_m+3 and T_m+6 and then a stabilization of κ for temperature above T_m+6, as shown in Figs. 20 and 21. These large drops of κ found close to the main phase transition temperature suggest anomalies near T_m, which may lead to a softening of the lipid bilayer. Hønger *et al.* [90] explained the anomalous swelling behavior in the phase transition region, which they observed experimentally by SANS measurements on multilamellar phospholipid bilayer systems, in terms of a thermal renormalization of the bilayer bending rigidity. This softening is thus caused by a

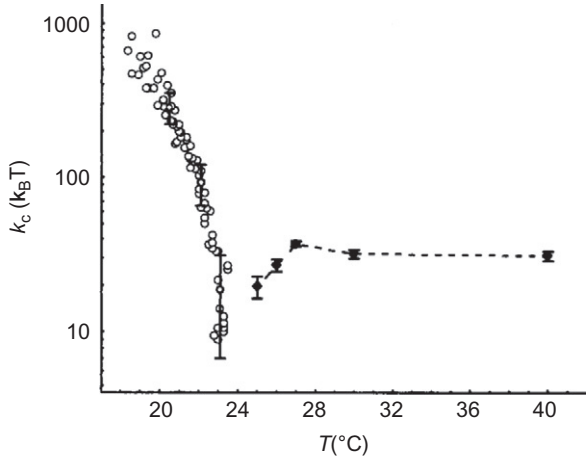

Figure 20 Thermal behavior of the DMPC membrane curvature modulus, adapted from Ref. [107]. The values of k_c in gel state (empty circles) were deduced from k_M in Ref. [107], while the values of k_c for fluid DMPC vesicles (diamond) were taken from Ref. [81]. The gel-to-liquid phase transition temperature for DMPC is equal to 23.9 °C [111].

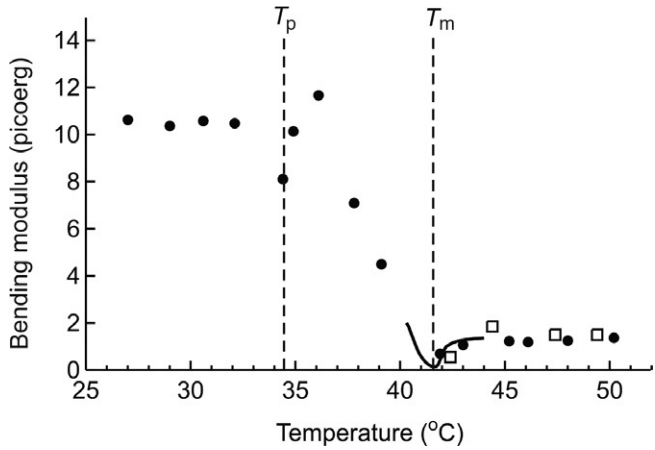

Figure 21 Bending elastic modulus of a DPPC vesicle as a function of the temperature [109]. Closed circles are data obtained from the confocal microscopy technique in Ref. [109] and open squares are data obtained from thermal fluctuation study in Ref. [71].

fluctuating difference in lateral density in the two monolayers of the bilayer, as expressed in the thermally renormalized bending elastic modulus.

A similar dependence of the bending rigidity on the temperature in the fluid phase has been measured by Chu *et al.* [114] with DMPC bilayer as shown in Fig. 22. They also suggested that anomalous swelling was due to a

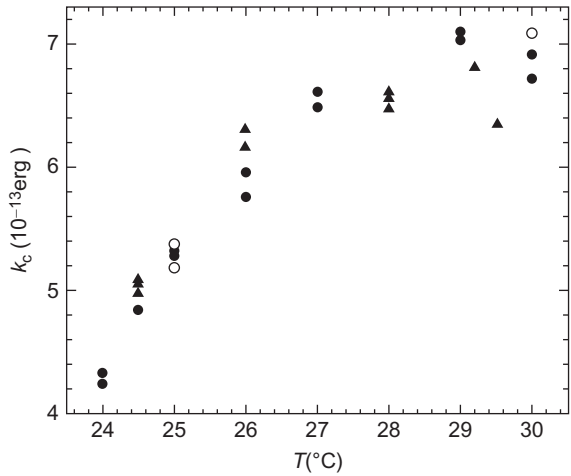

Figure 22 Effect of the temperature on the bending elasticity of DMPC bilayers [114] prepared using the rock-and-roll method [125]. The different symbols are due to different series of measurements and give thus a notion of the dispersion.

decrease of k_c, when the temperature decreased toward the main transition temperature T_m.

As for Pan *et al.* [126], they have not been interested in the anomalous swelling regime, but rather in the higher temperature behavior. A gradual decrease in k_c as the temperature increases is generally expected at higher temperatures, since the hydrocarbon core becomes both more fluid and thinner as a consequence of the increased disordering of the hydrocarbon chains. The experimental measurements of k_c for DOPC bilayers shown in Fig. 23A confirmed these expectations and demonstrated that the k_c modulus decreased with increasing temperature, according to a logarithmic dependence ($\ln k_c \propto (1/T)$) represented in Fig. 23B.

To summarize, it has been observed using different techniques that the bending rigidity decreased considerably near T_m on both sides of the transition, which was explained simply by the membrane becoming more flexible because each monolayer appeared to be more compressible. It was thus easy to locally bend the membrane by decreasing the density of the outside leaflet and increasing that of the inside one.

4.2. Dependence on the Chain Length and Saturation of the Lipid

The dependence of the bending rigidity on the molecular parameter of the lipid was first studied by Fernandez-Puente *et al.* [71] by focusing on the chain length of saturated phosphatidylcholine, whose results are displayed

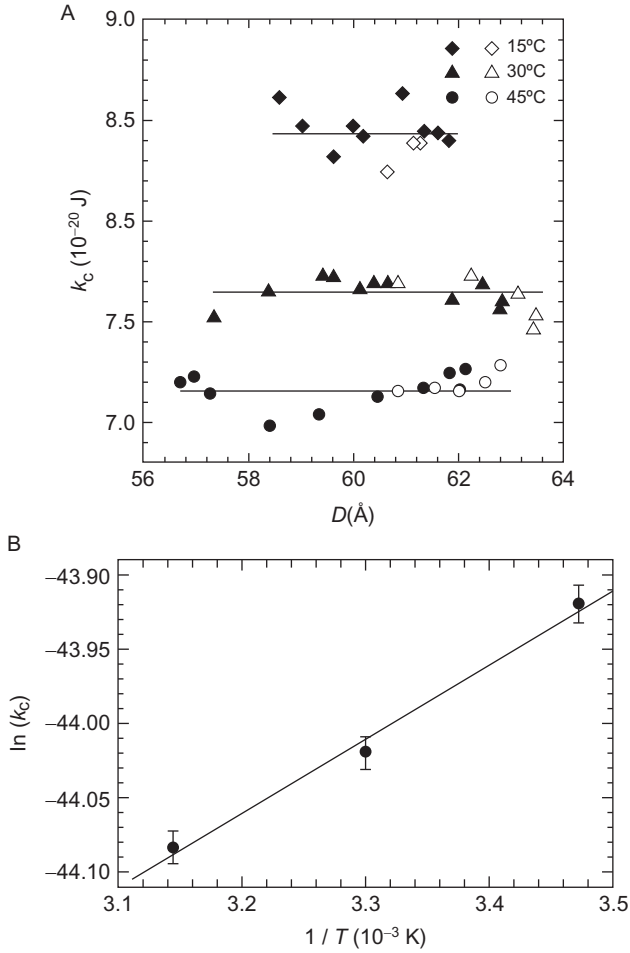

Figure 23 Effect of the temperature on the bending rigidity of DOPC bilayers obtained from X-ray study [126] prepared using the rock-and-roll method [125]. (A) Bending rigidity k_c versus lamellar repeat distance D, where the solid lines are the best k_c estimates for the three temperatures, and the open and solid symbols are from two different synchrotron trips on different beam lines. (B) Exponential plot for the bending modulus k_c.

Table 11 Bending rigidities obtained by studying the thermal fluctuations of GUVs at temperature above $T_m + 6$ [71]

Lipid	k_c ($\times 10^{-19}$ J)
DLPC	0.92 ± 0.05
DMPC	1.30 ± 0.08
DPPC	1.50 ± 0.09

in Table 11. A strong dependence of k_c on the lipid chain length was theoretically predicted using phenomenological descriptions [158] and conformational calculus [159,160]. These k_c measurements have shown that the bending rigidity scales as the square of the hydrophobic thickness of the bilayer, d_h, assuming a constant area per molecule, a, as displayed in Eq. (99) and shown in Fig. 24 [80].

$$k_c \sim \frac{d_h^2}{a} \tag{99}$$

Rawicz *et al.* [99] also demonstrated that the bending rigidity of saturated/monosaturated phosphatidylcholine lipids increased progressively with chain length from 0.56×10^{-19} J for diC13:0 to 1.2×10^{-19} J for diC22:1 (Table 12). Besides, the observed large decreases of the bending rigidity around 0.4×10^{-19} J for lipids with two or more alternating *cis*

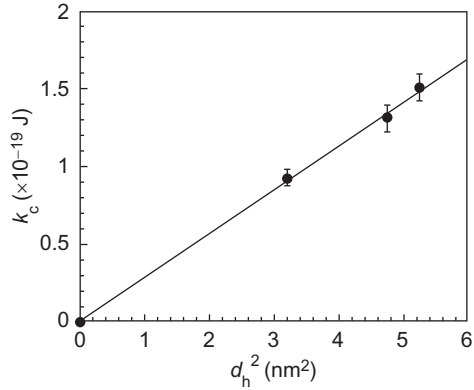

Figure 24 Comparison of the bending rigidities for DLPC, DMPC, and DPPC in the high temperature region as a function of the square of the hydrophobic length [80].

Table 12 Bending rigidities obtained using giant vesicles aspiration by micropipette at 18 °C (except for diC13:0 at 22 °C, for diC14:0 at 29 °C, and for diC22:1 at 21 °C) [99]

Lipid	k_c ($\times 10^{-19}$ J)	Lipid	k_c ($\times 10^{-19}$ J)
diC13:0	0.56 ± 0.07	diC18:1_{c6}	0.90 ± 0.09
diC14:0	0.56 ± 0.06	C18:0/2	0.46 ± 0.07
C18:0/1	0.90 ± 0.06	diC18:2	0.44 ± 0.07
C18:1/0	0.92 ± 0.07	diC18:3	0.38 ± 0.04
diC18:1_{c9}	0.85 ± 0.10	diC20:4	0.44 ± 0.05
diC18:1_{t9}	1.03 ± 0.11	diC22:1	1.20 ± 0.15

Giant vesicles were formed by gentle hydration in glucose/sucrose solution of 200 mOsm.

double bonds along one or both chains (C18:0/2, diC18:2, diC18:3, and diC20:4 in Table 12) indicated that poly-*cis* unsaturated chain bilayers were more flexible than saturated/monosaturated PC membranes.

A simulation from Stevens [133] also confirmed this tendency, namely, the variation of κ with the tail length, N_T being the varying number of hydrophobic beads constituting the lipid. For $N_T = 4$, 6, and 8, Stevens obtained $\kappa = 4$, 8, and 14 k_BT, respectively.

4.3. Effects of Various Molecules

Natural membranes are complex systems, composed systems, composed of a large number of components, as underlined previously in Section 1. It is thus interesting to understand how the chemical nature of the different membrane molecules governs the mechanical properties of these two-dimensional structures. Hence, several studies have performed systematic measurements of the bending rigidity of bilayers as a function of their composition or their environment.

4.3.1. Effect of sterols, mainly cholesterol

Mechanical properties of cholesterol containing bilayers have been studied extensively by several authors. In 1990, Duwe *et al.* [68] and Evans *et al.* [53], using flickering technique and micropipette technique, respectively, were the first ones to demonstrate that cholesterol induced a strong increase of the bending rigidity for PC bilayers (see Tables 4 and 6).

In 1997, Méléard *et al.* [81] performed a precise investigation of the effect of cholesterol on DMPC bilayers at different temperatures and molar ratios, whose results are displayed in Table 13.

Table 13 Bending rigidities of DMPC/cholesterol membranes obtained by studying the thermal fluctuations of GUVs [81]

Temperature (°C)	$k_c^{100/0}$ ($\times 10^{-19}$ J)	$k_c^{90/10}$ ($\times 10^{-19}$ J)	$k_c^{70/30}$ ($\times 10^{-19}$ J)	$k_c^{50/50}$ ($\times 10^{-19}$ J)
20			6.1 ± 0.2	
24.8		0.9 ± 0.2		
25	0.8 ± 0.13			
25.2			1.45 ± 0.06	
26	1.1 ± 0.1	1.63 ± 0.07		
27	1.52 ± 0.06	2.23 ± 0.07		
30	1.30 ± 0.08	2.00 ± 0.1	4.1 ± 0.25	6.1 ± 0.3
40	1.27 ± 0.09	1.84 ± 0.09	3.07 ± 0.13	3.7 ± 0.3

The superscript of the bending elasticity indicates the DMPC/cholesterol molar ratio.

Henriksen *et al.* [78] also studied the cholesterol effect and extended their study to other sterol compounds, namely, lanosterol and ergosterol. A similar behavior was observed for all sterols, that is, an increase in the bending rigidity as displayed in Table 14. An universal behavior was noticed for these sterol–lipid systems leading to relations between the elastic moduli and the first moments of ^{2}H NMR spectra [161].

As for Pan *et al.* [119], they found that the effect of cholesterol depended on the lipid composition, namely, that the effect of cholesterol on the bending rigidity increased with the number of saturated chains in the lipid as illustrated in Fig. 25. The bending rigidity remained essentially constant for two lipids that had both their chains mono-unsaturated, such as DOPC and diC22:1, while the bending elastic modulus with 30% cholesterol

Table 14 Bending rigidity values in k_BT units measured in the presence of various kinds of sterols and obtained by studying the thermal fluctuations of POPC giant unilamellar vesicles stabilized by gravity at 25 °C [78]

Sterol (mol%)	Cholesterol	Lanosterol	Ergosterol
10	54.4 ± 1.4	51.7 ± 1.2	45.8 ± 1.1
20	70.2 ± 0.8	61.3 ± 1.1	53.5 ± 1.7
30	86.8 ± 1.4	71.5 ± 0.6	54.6 ± 1.1

The k value for pure POPC bilayer is $(38.5 \pm 0.8)\,k_BT$.

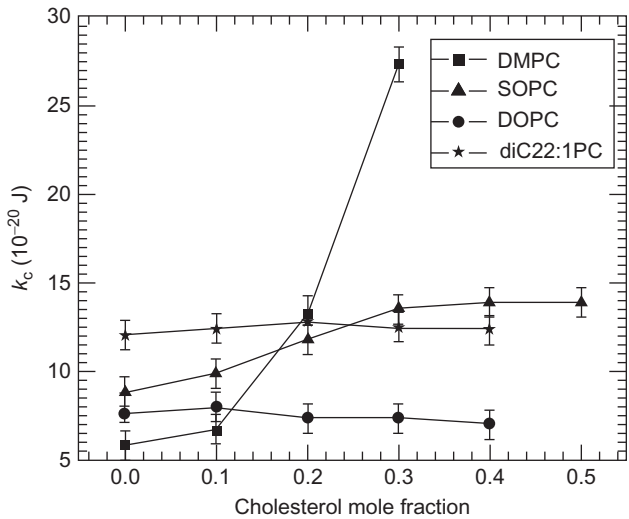

Figure 25 Effect of cholesterol on various lipids, adapted from Ref. [119]. The bending rigidities are obtained from X-ray measurements at 30 °C.

increased more than fourfold for saturated DMPC and only about twofold for SOPC, a lipid with one mono-unsaturated chain. The influence of the degree of saturation of the lipid host bilayer for the cholesterol effect has also been explored by Gracià *et al.* [76]. They confirmed the observation of Pan *et al.* with DOPC and further they noticed that the bending rigidity decreased for sphingomyelin membrane in the presence of cholesterol.

4.3.2. Effect of salts

Despite the intensive use of salts in most of the biophysical studies, very little is known regarding their effect on the bending rigidity. A study from Petrache *et al* [121], who looked at the effect of 1 M KCl and 0.1 M KBr for DLPC bilayers, did not show any significant changes of k_c with salt.

Recently, a careful study of the effect of various sodium salt from Bouvrais *et al.* [65] was performed and showed that the bending elastic modulus was strongly affected by the presence of sodium salts in the concentration range from 0 to 100 mM. These measurements indicated an ion specificity and a salt concentration dependence on the bending rigidity as shown in Table 15. The observation of major decreases in κ for the different sodium salts suggested that the ions were interfacially active in a specific way depending on their size and polarizability and this resulted in a softening of the lipid bilayer. A scaling of the bending rigidity decrease with the square root of the salt concentration was observed for all the sodium salt studied, as illustrated with the sodium thiocyanate in Fig. 26. This study highlighted the importance of salts for simple lipid bilayer and indicated that the bending rigidity could be added to the already long list of

Table 15 Bending rigidities in k_BT units obtained by study of the flickering of POPC GUVs in the presence of various sodium salt solutions at 22 °C [65]

Salt/Conc.	1 mM	4 mM	10 mM
NaCl	36.27 ± 1.01 (8)	32.54 ± 0.44 (9)	31.93 ± 1.03 (10)
NaBr	35.72 ± 0.77 (9)	33.53 ± 0.81 (11)	29.85 ± 0.70 (10)
NaI	37.73 ± 1.11 (8)	–	31.63 ± 0.71 (10)
NaSCN	36.36 ± 0.15 (9)	–	34.42 ± 1.19 (8)
Salt/Conc.	**50 mM**	**100 mM**	**250 mM**
NaF	–	32.99 ± 0.94 (5)	–
NaCl	–	31.01 ± 0.82 (9)	–
NaBr	–	29.15 ± 0.58 (10)	–
NaI	27.34 ± 1.84 (6)	27.58 ± 1.13 (8)	–
NaSCN	28.55 ± 1.19 (4)	24.54 ± 0.93 (10)	25.13 ± 0.60 (11)

Notice that the κ value without salt is equal to $(39.52 \pm 0.77)\, k_BT$. Error represents the standard deviation among a population of vesicle, whose number is indicated in parenthesis.

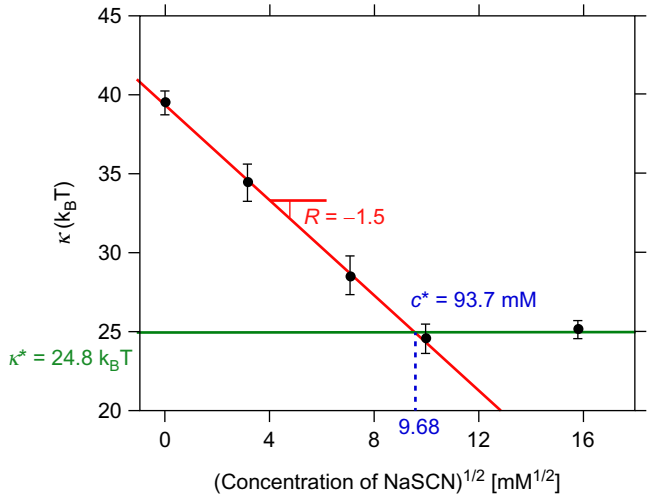

Figure 26 Scaling of the κ decrease with the square root of NaSCN concentration [65]. κ values are obtained from flickering measurements of GUVs. c^* indicates the concentration of saturation, κ^* the bending rigidity of saturation, and R the slope of the κ decrease for the lowest concentrations.

Table 16 Bending rigidities obtained by studying the thermal fluctuations of GUVs at room temperature [80]

Bilayer composition (mol ratio%)	k_c ($\times 10^{-19}$ J)
DLPC	0.91 ± 0.05
DLPC/DLPA (98/2)	0.92 ± 0.05
DLPC/DLPA (90/10)	1.05 ± 0.06
DLPC/DLPA (80/20)	1.06 ± 0.06

physicochemical parameters that suggest an ordering of ions according to the Hofmeister series.

4.3.3. Effect of charged molecules

After a first study from Song and Waugh [162] showing no significant difference in the bending rigidity values of systems composed of SOPC and SOPC/POPS (2 and 16 mol%), the role of surface charge on the bending rigidity was studied experimentally by Méléard *et al.* [80] using DLPC/DLPA mixtures with no added salt, where the surface charge depended on the PA molecular ratio. The results displayed in Table 16 show that the bending elastic modulus increased with the percentage of PA within the bilayer.

This was qualitatively in agreement with theoretical predictions from Andelman [163], but the charge-induced increase of the bending rigidity was modest in comparison to the quantitative theoretical expectations.

Rowat *et al.* [156] were able to isolate the electrostatic contribution to the bending rigidity by looking at the effects of ionic and nonionic surfactants with identical apolar chains (family of farnesylated peptides) for DMPC GUVs in the absence of additional salt (Table 17). The surface charge density resulted from the adsorption of ionic surfactants and this led to a significant enhancement of the bending rigidity of 3–5 k_BT due to charge effects, in good agreements with theoretical estimates (for reviews, see Refs. [163,164]).

4.4. Ability for an Amphipathic Helix to Locally Bend the Membrane

Magainin 2 is an antimicrobial peptide that interacts with the lipid membrane having the conformation of an α-helix. This helix is amphipathic and at low concentration lies parallel on the bilayer surface, with its hydrophobic residues buried into one of the monolayers of the lipid bilayer structure. Measurements of the bending rigidity of POPC GUVs in the symmetrical presence of magainin 2 enabled to investigate the physical perturbations induced by magainin 2 on the membrane [66]. A dramatic decrease of the bending rigidity as a function of the peptide concentration has been observed, indicating that magainin induced a softening of the lipid bilayer.

A simple continuum model describing the effects of peripheral inclusions on membrane stability has been developed, this model taking into account the local membrane curvature induced by the inclusions and the interactions between inclusions within the same monolayer and from opposite monolayers. This led to Eq. (100), which is the expression of the effective bending rigidity κ^{eff}, that is, the bending rigidity measured in the presence of inclusions.

Table 17 Bending rigidities of DMPC GUVs containing uncharged and charged surfactants at 37 °C obtained by flickering experiments [156]

Peptide	Bilayer composition (mol ratio%)	k_c ($\times 10^{-19}$ J)
	DMPC	1.40 ± 0.03
Uncharged	Ac-C-(farnesyl)-OMe (5 mol%)	1.32 ± 0.07
	Farnesol (2.5 mol%)	1.34 ± 0.03
	Farnesol (5 mol%)	1.34 ± 0.04
	Farnesol (25 mol%)	1.30 ± 0.05
Charged	Ac-NKNC-(farnesyl)-OMe (2.5 mol%)	1.60 ± 0.08
	Ac-NKNC-(farnesyl)-OMe (5 mol%)	1.59 ± 0.03
	Ac-NKNC-(farnesyl)-NH_2 (5 mol%)	1.72 ± 0.03

$$\kappa^{\text{eff}} = \kappa - \frac{4\lambda^2 \cdot \rho_0 / k_B T}{1 + (t - s) \cdot \rho_0 / k_B T} \tag{100}$$

with λ the parameter of coupling between the local shape of the membrane and the in-plane peptide distribution, t the parameter for the in-plane effective interactions between peptides within the monolayers, s the strength for the intermonolayer effective interactions between peptides, and ρ_0 the peptide density (see inset of Fig. 27 for a sketch of the interactions).

The characteristic experimentally observed dependence of κ^{eff} on the peptide density ρ_0 in the membrane has been fitted according to Eq. (100), which gave the following values: $\lambda = (3.19 \pm 0.37) \times 10^{-28}$ J·m and $(t - s) = (4.45 \pm 0.09) \times 10^{-36}$ J·m^2, as shown in Fig. 27.

The obtained value of the coupling parameter λ corresponded to a high local mean curvature, (a few nm)$^{-1}$. This left a picture of the membrane softening ability of magainin as originating from formation of local, mobile high-curvature spots on the membrane as sketched in Fig. 28. The observed saturation of κ^{eff} with increasing peptide coverage of the membrane made the estimate of $(t - s)$ relatively large and positive. As the in-plane interactions were dominated by contact interactions ($t \sim \pm 10^{-38}$ J·m^2), this suggested

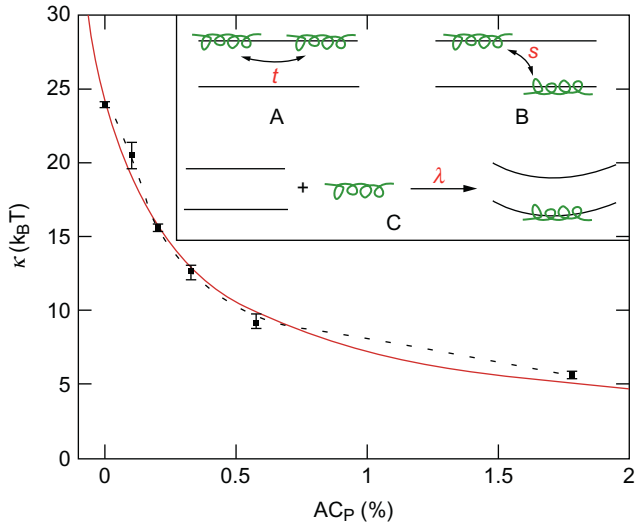

Figure 27 Comparison between the experimental decrease of the bending rigidity κ at 30 °C as a function of the peptide area coverage AC_p (data point) and a theoretical one (continuous line), for which $\lambda = (3.19 \pm 0.37) \times 10^{-28}$ J·m and $(t - s) = (4.45 \pm 0.09) \times 10^{-36}$ J·m^2. Inset, illustrations of the three phenomenological parameters of peptide/peptide and peptide/membrane interactions.

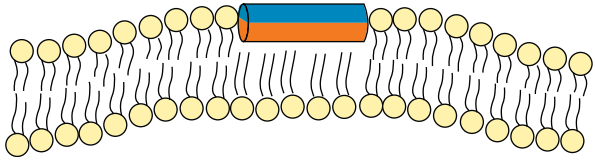

Figure 28 A cartoon of the effect of an α-helix insertion on the lipid packing [66]. The amphipathic character of the helix is illustrated with the color change (blue for the hydrophilic part and red for the hydrophobic one).

significant effective intermonolayer attractive associations $s \sim -10^{-36}\,\mathrm{J \cdot m^2}$, which partially restored the local symmetry between the monolayers.

Therefore, these κ measurements together with the modeling gave a picture of magainin inducing highly mobile regions with high curvature on the membrane surface, which softened the membrane and had some associations across the monolayers.

5. Conclusion

The present chapter focuses on the bending rigidity, a fundamental mechanical property characterizing how easily a membrane may deform at constant surface area. Some biophysical studies have consisted in measuring the bending rigidity as a function of changes in the biological systems, which were usually simplified membrane models such as lipid bilayers containing only a few components.

Different methods to determine the bending rigidity have been developed since the mid 1970s. Depending on the purpose of the study and the conditions, one technique may appear better than the other one. However, it can be noticed that the most used technique is the flickering experiment, which consists of monitoring by light microscopy the membrane fluctuations of a GUV as a function of time, whose amplitudes enable to get κ using the angular autocorrelation function and Helfrich's free energy, which describes the shape of a vesicle. Knowing that the shape fluctuations of the membranes play major roles in many biological processes (for instance, the RBCs are able to undergo major changes in their shapes allowing them to go through capillaries, whose diameters are smaller than their own size), it is natural to use as a first choice the flickering technique to obtain κ as a noninvasive method. The well-developed theory for the analysis of the fluctuations of quasispherical vesicles is based on the spherical harmonics: initially the averages of the fluctuations were used to get κ and later the analysis of the statistics of the membrane fluctuations has been performed leading to more precision in the determination of the bending rigidity.

The bending elastic modulus is acknowledged to depend strongly on the organization of the lipid bilayers, and thus the observed changes in the bending elastic modulus induced by additives or environmental modifications might give precious information on the nature of the interactions between lipids and additives. This property has been used in many biophysical studies so far. For example, the bending rigidity was shown to depend on the temperature decrease when approaching the fluid-to-gel main phase transition [71,81,107,109], the organization of the aliphatic region of the bilayer (the chain length and degree of saturation of the synthetic phosphatidylcholine) [71,99], the sterol content [78,81,119], or the characteristics of the head region with charge effects [80,156]. Consequently, this parameter has been a good candidate to reflect any changes in the organization of the main lipid component induced by the addition or the presence of an external component, such as the impact of membrane additives in the host bilayer, for example, antimicrobial peptides [66,87,92], fluorescent probes [67], lysolipids [77] or triglycerides [82], or the influence of the environment composed of various kinds of salts at different concentrations [65].

REFERENCES

[1] B. Alberts, D. Bray, J. Lewis, M. Raff, K. Roberts, J.D. Watson, Molecular Biology of the Cell, Garland Publishing, New York, 1994.
[2] E. Sackmann, Biological membranes architecture and function, in: R. Lipowsky, E. Sackmann (Eds.), Handbook of Biological Physics vol. 1A Elsevier Science B.V, Amsterdam, Chapter 1, 1995.
[3] T. Heimburg, Thermal Biophysics of Membranes, Wiley-VCH, Weinheim, 2007.
[4] O.G. Mouritsen, Life—As a Matter of Fat: The Emerging Science of Lipodomics, Springer-Verlag, Heidelberg, 2005.
[5] G.A. Jamieson, D.M. Robinson, Mammalian Cell Membranes: Responses of Plasma Membranes, Butterworths, London, 1977.
[6] E. Gorter, F. Grendel, On bimolecular layers of lipids on the chromocytes of the blood, J. Exp. Med. 41(4) (1925) 439.
[7] H.A. Davson, J.F. Danielli, A contribution to the theory of thin films, J. Cell. Comp. Physiol. 5 (1935) 495–508.
[8] J.D. Robertson, New observations on the ultrastructure of the membranes of frog peripheral nerve fibers, J. Cell Biol. 3(6) (1957) 1043.
[9] S.J. Singer, G.L. Nicolson, The fluid mosaic model of the structure of cell membranes, Science 175(4023) (1972) 720–731.
[10] J.N. Israelachvili, A.C.T. Canberra, The packing of lipids and proteins in membranes, in: D.W. Deamer (Ed.), Light Transducing Membranes: Structure Function and Evolution pages, Academic Press, New York, 1978, pp. 91–107.
[11] O.G. Mouritsen, M. Bloom, Mattress model of lipid-protein interactions in membranes, Biophys. J. 46(2) (1984) 141–153.
[12] S. Mayor, M. Rao, Rafts: scale-dependent, active lipid organization at the cell surface, Traffic 5(4) (2004) 231–240.
[13] L.J. Pike, Rafts defined: a report on the Keystone symposium on lipid rafts and cell function, J. Lipid Res. 47(7) (2006) 1597.

[14] K. Simons, E. Ikonen, Functional rafts in cell membranes, Nature 387(6633) (1997) 569–572.
[15] E. Sackmann, Supported membranes: scientific and practical applications, Science 271 (5245) (1996) 4343.
[16] L.K. Tamm, H.M. McConnell, Supported phospholipid bilayers, Biophys. J. 47 (1) (1985) 105–113.
[17] K. Akashi, H. Miyata, H. Itoh, K. Kinosita, Preparation of giant liposomes in physiological conditions and their characterization under an optical microscope, Biophys. J. 71(6) (1996) 3242–3250.
[18] D.D. Lasic, Liposomes: From Physics to Applications, Elsevier Science Ltd, Amsterdam, 1993.
[19] A. Lorin, C. Flore, A. Thomas, R. Brasseur, Les liposomes: description, fabrication et applications, Biotechnol. Agron. Soc. Environ. 8(3) (2004) 163–176.
[20] P.L. Luisi, P. Walde, Giant Vesicles, Wiley, Chichester, 2000.
[21] F.M. Menger, J.S. Keiper, Chemistry and physics of giant vesicles as biomembrane models, Curr. Opin. Chem. Biol. 2(6) (1998) 726–732.
[22] P. Walde, K. Cosentino, H. Engel, P. Stano, Giant vesicles: preparations and applications, Chembiochem 11(7) (2010) 834.
[23] J.P. Reeves, R.M. Dowben, Formation and properties of thin-walled phospholipid vesicles, J. Cell. Physiol. 73(1) (1969) 49–60.
[24] E.E. Ambroggio, F. Separovic, J.H. Bowie, G.D. Fidelio, L.A. Bagatolli, Direct visualization of membrane leakage induced by the antibiotic peptides: maculatin, citropin, and aurein, Biophys. J. 89(3) (2005) 1874–1881.
[25] L.A. Bagatolli, S.A. Sanchez, T. Hazlett, E. Gratton, Giant vesicles, laurdan, and two-photon fluorescence microscopy: evidence of lipid lateral separation in bilayers, Methods Enzymol. 360 (2003) 481–500.
[26] T. Baumgart, S.T. Hess, W.W. Webb, Imaging coexisting fluid domains in biomembrane models coupling curvature and line tension, Nature 425(6960) (2003) 821–824.
[27] R. Dimova, S. Aranda, N. Bezlyepkina, V. Nikolov, K.A. Riske, R. Lipowsky, A practical guide to giant vesicles. Probing the membrane nanoregime via optical microscopy, J. Phys. Condens. Matter 18 (2006) S1151–S1176.
[28] A. Fischer, T. Oberholzer, P.L. Luisi, Giant vesicles as models to study the interactions between membranes and proteins, Biochim. Biophys. Acta Biomembr. 1467 (1) (2000) 177–188.
[29] J. Korlach, C. Reichle, T. Müller, T. Schnelle, W.W. Webb, Trapping, deformation, and rotation of giant unilamellar vesicles in octode dielectrophoretic field cages, Biophys. J. 89(1) (2005) 554–562.
[30] G. Staneva, M. Seigneuret, K. Koumanov, G. Trugnan, M.I. Angelova, Detergents induce raft-like domains budding and fission from giant unilamellar heterogeneous vesicles: a direct microscopy observation, Chem. Phys. Lipids 136(1) (2005) 55–66.
[31] O. Wesołowska, K. Michalak, J. Maniewska, A.B. Hendrich, Giant unilamellar vesicles—a perfect tool to visualize phase separation and lipid rafts in model systems, Acta Biochim. Pol. 56(1) (2009) 33–39.
[32] M.I. Angelova, D.S. Dimitrov, Liposome electroformation, Faraday Discuss. Chem. Soc. 81 (1986) 303–311.
[33] M.I. Angelova, S. Soleau, P. Méléard, J.F. Faucon, P. Bothorel, Preparation of giant vesicles by external AC electric fields. Kinetics and applications, Progr. Colloid Polym. Sci. 89 (1992) 127–131.
[34] L.A. Bagatolli, E. Gratton, T.K. Khan, P.L.G. Chong, Two-photon fluorescence microscopy studies of bipolar tetraether giant liposomes from thermoacidophilic archaebacteria Sulfolobus acidocaldarius, Biophys. J. 79(1) (2000) 416–425.

[35] J. Bernardino de la Serna, J. Perez-Gil, A.C. Simonsen, L.A. Bagatolli, Cholesterol rules: direct observation of the coexistence of two fluid phases in native pulmonary surfactant membranes at physiological temperatures, J. Biol. Chem. 279 (2004) 40715–40722.
[36] C. Dietrich, L.A. Bagatolli, Z.N. Volovyk, N.L. Thompson, M. Levi, K. Jacobson, et al.Lipid rafts reconstituted in model membranes, Biophys. J. 80(3) (2001) 1417–1428.
[37] K. Nag, J.S. Pao, R.R. Harbottle, F. Possmayer, N.O. Petersen, L.A. Bagatolli, Segregation of saturated chain lipids in pulmonary surfactant films and bilayers, Biophys. J. 82(4) (2002) 2041–2051.
[38] T. Baumgart, A.T. Hammond, P. Sengupta, S.T. Hess, D.A. Holowka, B.A. Baird, et al.Large-scale fluid/fluid phase separation of proteins and lipids in giant plasma membrane vesicles, Proc. Natl. Acad. Sci. USA 104(9) (2007) 3165.
[39] L.R. Montes, A. Alonso, F.M. Goñi, L.A. Bagatolli, Giant unilamellar vesicles electroformed from native membranes and organic lipid mixtures under physiological conditions, Biophys. J. 93(10) (2007) 3548–3554.
[40] Q. Ruan, M.A. Cheng, M. Levi, E. Gratton, W.W. Mantulin, Spatial-temporal studies of membrane dynamics: scanning fluorescence correlation spectroscopy (SFCS), Biophys. J. 87(2) (2004) 1260–1267.
[41] P. Girard, J. Pécréaux, G. Lenoir, P. Falson, J.L. Rigaud, P. Bassereau, A new method for the reconstitution of membrane proteins into giant unilamellar vesicles, Biophys. J. 87(1) (2004) 419–429.
[42] N. Kahya, E.I. Pécheur, W.P. de Boeij, D.A. Wiersma, D. Hoekstra, Reconstitution of membrane proteins into giant unilamellar vesicles via peptide-induced fusion, Biophys. J. 81(3) (2001) 1464–1474.
[43] A. Moscho, O. Orwar, D.T. Chiu, B.P. Modi, R.N. Zare, Rapid preparation of giant unilamellar vesicles, Proc. Natl. Acad. Sci. USA 93(21) (1996) 11443.
[44] T. Pott, H. Bouvrais, P. Méléard, Giant unilamellar vesicle formation under physiologically relevant conditions, Chem. Phys. Lipids 154(2) (2008) 115–119.
[45] R.C. MacDonald, R.I. MacDonald, B.P.M. Menco, K. Takeshita, N.K. Subbarao, L. Hu, Small-volume extrusion apparatus for preparation of large, unilamellar vesicles, Biochim. Biophys. Acta Biomembr. 1061(2) (1991) 297–303.
[46] L.D. Mayer, M.J. Hope, P.R. Cullis, Vesicles of variable sizes produced by a rapid extrusion procedure, Biochim. Biophys. Acta Biomembr. 858(1) (1986) 161–168.
[47] B. Mui, L. Chow, M.J. Hope, Extrusion technique to generate liposomes of defined size, Methods Enzymol. 367 (2003) 3.
[48] F. Szoka, D. Papahadjopoulos, Procedure for preparation of liposomes with large internal aqueous space and high capture by reverse-phase evaporation, Proc. Natl. Acad. Sci. USA 75(9) (1978) 4194.
[49] C.H. Huang, Phosphatidylcholine vesicles. Formation and physical characteristics, Biochemistry 8(1) (1969) 344–352.
[50] D. Papahadjopoulos, N. Miller, Phospholipid model membranes. I. Structural characteristics of hydrated liquid crystals, Biochim. Biophys. Acta Biomembr. 135 (4) (1967) 624–638.
[51] M.P. Sheetz, S.I. Chan, Effect of sonication on the structure of lecithin bilayers, Biochemistry 11(24) (1972) 4573–4581.
[52] J.L. Rigaud, D. Levy, Reconstitution of membrane proteins into liposomes, Methods Enzymol. 372 (2003) 65.
[53] E. Evans, W. Rawicz, Entropy-driven tension and bending elasticity in condensed-fluid membranes, Phys. Rev. Lett. 64(17) (1990) 2094–2097.
[54] W. Helfrich, Elastic properties of lipid bilayers: theory and possible experiments, Z. Naturforsch. 28c(11) (1973) 693–703.

[55] E. Sackmann, Membrane bending energy concept of vesicle-and cell-shapes and shape-transitions, FEBS Lett. 346(1) (1994) 3–16.
[56] H.J. Deuling, W. Helfrich, Red blood cell shapes as explained on the basis of curvature elasticity, Biophys. J. 16(8) (1976) 861–868.
[57] H.J. Deuling, W. Helfrich, The curvature elasticity of fluid membranes: a catalogue of vesicle shapes, J. Phys. 37(11) (1976) 1335–1345.
[58] F. Brochard, J.F. Lennon, Frequency spectrum of the flicker phenomenon in erythrocytes, J. Phys. (Paris) 36 (1975) 1035–1047.
[59] T. Browicz, Further observation of motion phenomena on red blood cells in pathological states, Zbl. med. Wissen 28 (1890) 625–627.
[60] G. Beblik, R.M. Servuss, W. Helfrich, Bilayer bending rigidity of some synthetic lecithins, J. Phys. (Paris) 46(10) (1985) 1773–1778.
[61] M.B. Schneider, J.T. Jenkins, W.W. Webb, Thermal fluctuations of large cylindrical phospholipid vesicles, Biophys. J. 45(5) (1984) 891–899.
[62] R.M. Servuss, W. Harbich, W. Helfrich, Measurement of the curvature-elastic modulus of egg lecithin bilayers, Biochim. Biophys. Acta 436(4) (1976) 900–903.
[63] M. Mutz, W. Helfrich, Bending rigidities of some biological model membranes as obtained from the Fourier analysis of contour sections, J. Phys. (Paris) 51(10) (1990) 991–1001.
[64] I. Bivas, P. Hanusse, P. Bothorel, J. Lalanne, O. Aguerre-Chariol, An application of the optical microscopy to the determination of the curvature elastic modulus of biological and model membranes, J. Phys. (Paris) 48(5) (1987) 855–867.
[65] H. Bouvrais, P. Méléard, T. Pott, J.H. Ipsen. Anion specificity of sodium salts on the bending rigidity of POPC lipid bilayer, 2012, in preparation.
[66] H. Bouvrais, P. Méléard, T. Pott, K.J. Jensen, J. Brask, J.H. Ipsen, Softening of POPC membranes by magainin, Biophys. Chem. 137(1) (2008) 7–12.
[67] H. Bouvrais, T. Pott, L.A. Bagatolli, J.H. Ipsen, P. Méléard, Impact of membrane-anchored fluorescent probes on the mechanical properties of lipid bilayers, Biochim. Biophys. Acta Biomembr. 1798(7) (2010) 1333–1337.
[68] H.P. Duwe, J. Kaes, E. Sackmann, Bending elastic moduli of lipid bilayers: modulation by solutes, J. Phys. (Paris) 51(10) (1990) 945–961.
[69] H. Engelhardt, H.P. Duwe, E. Sackmann, Bilayer bending elasticity measured by Fourier analysis of thermally excited surface undulations of flaccid vesicles, J. Phys. Lett. 46(8) (1985) 395–400.
[70] J.F. Faucon, M.D. Mitov, P. Méléard, I. Bivas, P. Bothorel, Bending elasticity and thermal fluctuations of lipid membranes. Theoretical and experimental requirements, J. Phys. (France) 50 (1989) 2389–2414.
[71] L. Fernandez-Puente, I. Bivas, M.D. Mitov, P. Méléard, Temperature and chain length effects on bending elasticity of phosphatidylcholine bilayers, Europhys. Lett. 28 (3) (1994) 181–186.
[72] J. Genova, V. Vitkova, L. Aladgem, P. Méléard, M.D. Mitov, Using stroboscopic illumination to improve the precision of the bending modulus measurement, Bulg. J. Phys. 31(1–2) (2004) 68–75.
[73] J. Genova, V. Vitkova, L. Aladjem, P. Méléard, M.D. Mitov, Stroboscopic illumination gives new opportunities and improves the precision of bending elastic modulus measurements, J. Optoelectron. Adv. Mater. 7(1) (2005) 257–260.
[74] J. Genova, A. Zheliaskova, M.D. Mitov, Monosaccharides (fructose, glucose) and disaccharides (sucrose, trehalose) influence the elasticity of SOPC membranes, J. Optoelectron. Adv. Mater. 9(2) (2007) 427–430.
[75] J. Genova, A. Zheliaskova, M.D. Mitov, Does maltose influence on the elasticity of SOPC membrane? J. Phys. Conf. Ser. 253 (2010) 012063.

[76] R.S. Gracià, N. Bezlyepkina, R.L. Knorr, R. Lipowsky, R. Dimova, Effect of cholesterol on the rigidity of saturated and unsaturated membranes: fluctuation and electrodeformation analysis of giant vesicles, Soft Matter 6(7) (2010) 1472–1482.
[77] J.R. Henriksen, T.L. Andresen, L.N. Feldborg, L. Duelund, J.H. Ipsen, Understanding detergent effects on lipid membranes: a model study of lysolipids, Biophys. J. 98 (10) (2010) 2199.
[78] J.R. Henriksen, A.C. Rowat, J.H. Ipsen, Vesicle fluctuation analysis of the effects of sterols on membrane bending rigidity, Eur. Biophys. J. 33(8) (2004) 732–741.
[79] P. Méléard, J.F. Faucon, M.D. Mitov, P. Bothorel, Pulsed-light microscopy applied to the measurement of the bending elasticity of giant liposomes, Europhys. Lett. 19 (4) (1992) 267–271.
[80] P. Méléard, C. Gerbeaud, P. Bardusco, N. Jeandaine, M.D. Mitov, L. Fernandez-Puente, Mechanical properties of model membranes studied from shape transformations of giant vesicles, Biochimie 80(5–6) (1998) 401–413.
[81] P. Méléard, C. Gerbeaud, T. Pott, L. Fernandez-Puente, I. Bivas, M.D. Mitov, et al. Bending elasticities of model membranes: influences of temperature and sterol content, Biophys. J. 72(6) (1997) 2616–2629.
[82] K.I. Pakkanen, L. Duelund, K. Qvortrup, J.S. Pedersen, J.H. Ipsen, Mechanics and dynamics of triglyceride-phospholipid model membranes: implications for cellular properties and function, Biochim. Biophys. Acta Biomembr. 1808 (2011) 1947–1956.
[83] J.I. Pavlič, J. Genova, A. Zheliaskova, A. Iglič, M.D. Mitov, Bending elasticity of lipid membranes in presence of beta 2 glycoprotein I in the surrounding solution, J. Phys. Conf. Ser. 253 (2010) 012064.
[84] J. Pécréaux, H.G. Döbereiner, J. Prost, J.F. Joanny, P. Bassereau, Refined contour analysis of giant unilamellar vesicles, Eur. Phys. J. E 13(3) (2004) 277–290.
[85] E. Sackmann, H.P. Duwe, H. Engelhardt, Membrane bending elasticity and its role for shape fluctuations and shape transformations of cells and vesicles, Faraday Discuss. Chem. Soc. 81 (1986) 281–290.
[86] M.B. Schneider, J.T. Jenkins, W.W. Webb, Thermal fluctuations of large quasi-spherical bimolecular phospholipid vesicles, J. Phys. (Paris) 45(9) (1984) 1457–1472.
[87] V. Vitkova, P. Méléard, T. Pott, I. Bivas, Alamethicin influence on the membrane bending elasticity, Eur. Biophys. J. 35(3) (2006) 281–286.
[88] M.D. Mitov, J.F. Faucon, P. Méléard, I. Bivas, P. Bothorel, Thermal fluctuations of membranes, in: G.W. Gokel (Ed.), Advances in Supramolecular Chemistry vol. 2 Jai Press, Greenwich, 1992, 93–139.
[89] M.I. Angelova, S. Soleau, P. Méléard, J.F. Faucon, P. Bothorel, AC field controlled formation of giant fluctuating vesicles and bending elasticity measurements, Springer Proc. Phys. 66 (1992) 178–182.
[90] T. Hønger, K. Mortensen, J.H. Ipsen, J. Lemmich, R. Bauer, O.G. Mouritsen, Anomalous swelling of multilamellar lipid bilayers in the transition region by renormalization of curvature elasticity, Phys. Rev. Lett. 72(24) (1994) 3911–3914.
[91] J.R. Henriksen, J.H. Ipsen, Thermal undulations of quasi-spherical vesicles stabilized by gravity, Eur. Phys. J. E 9(4) (2002) 365–374.
[92] C. Gerbeaud, Effet de l'insertion de protéines et de peptides membranaires sur les propriétés mécaniques et les changements morphologiques de vésicules géantes, Ph.D. Thesis, Université de Bordeaux I, 1998.
[93] W. Häckl, U. Seifert, E. Sackmann, Effects of fully and partially solubilized amphiphiles on bilayer bending stiffness and temperature dependence of the effective tension of giant vesicles, J. Phys. II, France 7 (1997) 1141–1157.
[94] H. Bouvrais, Mechanical properties of giant vesicle membranes investigated by flickering technique. Ph.D. Thesis, 2011, University of Southern Denmark.

[95] P. Méléard, T. Pott, H. Bouvrais, J.H. Ipsen, Statistical analysis of giant vesicle thermal fluctuations for bending elasticity measurements, Eur. Phys. J. E 34(11) (2011) 1–6.
[96] E. Evans, Bending elastic modulus of red blood cell membrane derived from buckling instability in micropipet aspiration tests, Biophys. J. 43(1) (1983) 27.
[97] E. Evans, D. Needham, Physical properties of surfactant bilayer membranes: thermal transitions, elasticity, rigidity, cohesion and colloidal interactions, J. Phys. Chem. 91 (16) (1987) 4219–4228.
[98] J.R. Henriksen, J.H. Ipsen, Measurement of membrane elasticity by micro-pipette aspiration, Eur. Phys. J. E Soft Matter 14(2) (2004) 149–167.
[99] W. Rawicz, K.C. Olbrich, T. McIntosh, D. Needham, E. Evans, Effect of chain length and unsaturation on elasticity of lipid bilayers, Biophys. J. 79(1) (2000) 328–339.
[100] L. Bo, R.E. Waugh, Determination of bilayer membrane bending stiffness by tether formation from giant, thin-walled vesicles, Biophys. J. 55(3) (1989) 509–517.
[101] D. Cuvelier, I. Derényi, P. Bassereau, P. Nassoy, Coalescence of membrane tethers: experiments, theory, and applications, Biophys. J. 88(4) (2005) 2714–2726.
[102] V. Heinrich, R.E. Waugh, A piconewton force transducer and its application to measurement of the bending stiffness of phospholipid membranes, Ann. Biomed. Eng. 24(5) (1996) 595–605.
[103] E.I. Settles, A.F. Loftus, A.N. McKeown, R. Parthasarathy, The vesicle trafficking protein sar1 lowers lipid membrane rigidity, Biophys. J. 99(5) (2010) 1539–1545.
[104] J. Song, R.E. Waugh, Bending rigidity of SOPC membranes containing cholesterol, Biophys. J. 64(6) (1993) 1967–1970.
[105] R.E. Waugh, R.M. Hochmuth, Mechanical equilibrium of thick, hollow, liquid membrane cylinders, Biophys. J. 52(3) (1987) 391.
[106] M. Kummrow, W. Helfrich, Deformation of giant lipid vesicles by electric fields, Phys. Rev. A 44(12) (1991) 8356–8360.
[107] R. Dimova, B. Pouligny, C. Dietrich, Pretransitional effects in dimyristoylphosphatidylcholine vesicle membranes: optical dynamometry study, Biophys. J. 79(1) (2000) 340–356.
[108] C.H. Lee, W.C. Lin, J. Wang, Measuring the bending rigidity of giant unilamellar liposomes with differential confocal microscopy, Lasers Electro Optics (2000) 592–593.
[109] C.H. Lee, W.C. Lin, J. Wang, All-optical measurements of the bending rigidity of lipid-vesicle membranes across structural phase transitions, Phys. Rev. E 64(2) (2001) 020901.
[110] C.H. Lee, J. Wang, Noninterferometric differential confocal microscopy with 2-nm depth resolution, Opt. Commun. 135(4–6) (1997) 233–237.
[111] R.N.A.H. Lewis, N. Mak, R.N. McElhaney, A differential scanning calorimetric study of the thermotropic phase behavior of model membranes composed of phosphatidylcholines containing linear saturated fatty acyl chains, Biochemistry 26 (19) (1987) 6118–6126.
[112] L.R. Arriaga, I. López-Montero, F. Monroy, G. Orts-Gil, B. Farago, T. Hellweg, Stiffening effect of cholesterol on disordered lipid phases: a combined neutron spin echo + dynamic light scattering analysis of the bending elasticity of large unilamellar vesicles, Biophys. J. 96(9) (2009) 3629–3637.
[113] L.R. Arriaga, I. López-Montero, G. Orts-Gil, B. Farago, T. Hellweg, F. Monroy, Fluctuation dynamics of spherical vesicles: frustration of regular bulk dissipation into subdiffusive relaxation, Phys. Rev. E 80(3) (2009) 031908.
[114] N. Chu, N. Kučerka, Y. Liu, S. Tristram-Nagle, J.F. Nagle, Anomalous swelling of lipid bilayer stacks is caused by softening of the bending modulus, Phys. Rev. E 71 (4) (2005) 41904.
[115] N. Kučerka, Y. Liu, N. Chu, H.I. Petrache, S. Tristram-Nagle, J.F. Nagle, Structure of fully hydrated fluid phase DMPC and DLPC lipid bilayers using X-Ray scattering

from oriented multilamellar arrays and from unilamellar vesicles, Biophys. J. 88(4) (2005) 2626–2637.
[116] N. Kučerka, S. Tristram-Nagle, J.F. Nagle, Structure of fully hydrated fluid phase lipid bilayers with monounsaturated chains, J. Membr. Biol. 208(3) (2006) 193–202.
[117] Y. Liu, J.F. Nagle, Diffuse scattering provides material parameters and electron density profiles of biomembranes, Phys. Rev. E 69(4) (2004) 40901.
[118] Y. Lyatskaya, Y. Liu, S. Tristram-Nagle, J. Katsaras, J.F. Nagle, Method for obtaining structure and interactions from oriented lipid bilayers, Phys. Rev. E 63(1) (2000) 11907.
[119] J. Pan, T.T. Mills, S. Tristram-Nagle, J.F. Nagle, Cholesterol perturbs lipid bilayers nonuniversally, Phys. Rev. Lett. 100(19) (2008) 198103.
[120] J. Pan, S. Tristram-Nagle, J.F. Nagle, Effect of cholesterol on structural and mechanical properties of membranes depends on lipid chain saturation, Phys. Rev. E 80 (2) (2009) 21931.
[121] H.I. Petrache, S. Tristram-Nagle, D. Harries, N. Kučerka, J.F. Nagle, V.A. Parsegian, Swelling of phospholipids by monovalent salt, J. Lipid Res. 47 (2006) 302–309.
[122] A. Zilker, H. Engelhardt, E. Sackmann, Dynamic reflection interference contrast (RIC-) microscopy: a new method to study surface excitations of cells and to measure membrane bending elastic moduli, J. Phys. (France) 48 (1987) 2139–2151.
[123] A. Zilker, M. Ziegler, E. Sackmann, Spectral analysis of erythrocyte flickering in the 0.3–4-μm^{-1} regime by microinterferometry combined with fast image processing, Phys. Rev. A 46(12) (1992) 7998.
[124] A. Caillé, Remarques sur la diffusion des rayons x dans les smectiques, C. R. Acad. Sci. Paris Ser. B 274 (1972) 891–893.
[125] S. Tristram-Nagle, R. Zhang, R.M. Suter, C.R. Worthington, W.J. Sun, J.F. Nagle, Measurement of chain tilt angle in fully hydrated bilayers of gel phase lecithins, Biophys. J. 64(4) (1993) 1097.
[126] J. Pan, S. Tristram-Nagle, N. Kučerka, J.F. Nagle, Temperature dependence of structure, bending rigidity, and bilayer interactions of Dioleoylphosphatidylcholine bilayers, Biophys. J. 94(1) (2008) 117.
[127] A.G. Zilman, R. Granek, Undulations and dynamic structure factor of membranes, Phys. Rev. Lett. 77(23) (1996) 4788–4791.
[128] R.D. Groot, P.B. Warren, Dissipative particle dynamics: bridging the gap between atomistic and mesoscopic simulation, J. Chem. Phys. 107(11) (1997) 4423.
[129] R. Goetz, G. Gompper, R. Lipowsky, Mobility and elasticity of self-assembled membranes, Phys. Rev. Lett. 82(1) (1999) 221–224.
[130] G. Ayton, G.A. Voth, Bridging microscopic and mesoscopic simulations of lipid bilayers, Biophys. J. 83(6) (2002) 3357–3370.
[131] S.J. Marrink, A.H. de Vries, A.E. Mark, Coarse grained model for semiquantitative lipid simulations, J. Phys. Chem. B 108(2) (2004) 750–760.
[132] E.R. May, A. Narang, D.I. Kopelevich, Role of molecular tilt in thermal fluctuations of lipid membranes, Phys. Rev. E 76(2) (2007) 21913.
[133] M.J. Stevens, Coarse-grained simulations of lipid bilayers, J. Chem. Phys. 121 (2004) 11942.
[134] A. Imparato, J.C. Shillcock, R. Lipowsky, Shape fluctuations and elastic properties of two-component bilayer membranes, Europhys. Lett. 69 (2005) 650.
[135] E.S. Boek, J.T. Padding, W.K. den Otter, W.J. Briels, Mechanical properties of surfactant bilayer membranes from atomistic and coarse-grained molecular dynamics simulations, J. Phys. Chem. B 109(42) (2005) 19851–19858.
[136] G. Brannigan, F.L.H. Brown, A consistent model for thermal fluctuations and protein-induced deformations in lipid bilayers, Biophys. J. 90(5) (2006) 1501–1520.

[137] I.R. Cooke, M. Deserno, Solvent-free model for self-assembling fluid bilayer membranes: stabilization of the fluid phase based on broad attractive tail potentials, J. Chem. Phys. 123 (2005) 224710.
[138] O. Farago, Water-free computer model for fluid bilayer membranes, J. Chem. Phys. 119 (2003) 596.
[139] E. Lindahl, O. Edholm, Mesoscopic undulations and thickness fluctuations in lipid bilayers from molecular dynamics simulations, Biophys. J. 79(1) (2000) 426–433.
[140] S.J. Marrink, A.E. Mark, Effect of undulations on surface tension in simulated bilayers, J. Phys. Chem. B 105(26) (2001) 6122–6127.
[141] S.W. Chiu, S. Vasudevan, E. Jakobsson, R.J. Mashl, H.L. Scott, Structure of sphingomyelin bilayers: a simulation study, Biophys. J. 85(6) (2003) 3624–3635.
[142] W.K. den Otter, W.J. Briels, The bending rigidity of an amphiphilic bilayer from equilibrium and nonequilibrium molecular dynamics, J. Chem. Phys. 118 (2003) 4712.
[143] O. Farago, P. Pincus, Statistical mechanics of bilayer membrane with a fixed projected area, J. Chem. Phys. 120 (2004) 2934.
[144] V.A. Harmandaris, M. Deserno, A novel method for measuring the bending rigidity of model lipid membranes by simulating tethers, J. Chem. Phys. 125 (2006) 204905.
[145] S. Baoukina, L. Monticelli, H.J. Risselada, S.J. Marrink, D.P. Tieleman, The molecular mechanism of lipid monolayer collapse, Proc. Natl. Acad. Sci. USA 105 (31) (2008) 10803.
[146] J. Wong-Ekkabut, S. Baoukina, W. Triampo, I.M. Tang, D.P. Tieleman, L. Monticelli, Computer simulation study of fullerene translocation through lipid membranes, Nat. Nanotechnol. 3(6) (2008) 363–368.
[147] H.G. Döbereiner, G. Gompper, C.K. Haluska, D.M. Kroll, P.G. Petrov, K.A. Riske, Advanced flicker spectroscopy of fluid membranes, Phys. Rev. Lett. 91(4) (2003) 48301.
[148] N. Fa, Micro-rhéologie de vésicules géantes, Ph.D. Thesis, Université de Strasbourg, 2003.
[149] P. Girard, Membranes hors d'équilibre: échanges et transport actif, Ph.D. Thesis, Université de Paris 7, 2004.
[150] G. Niggemann, M. Kummrow, W. Helfrich, The bending rigidity of phosphatidylcholine bilayers: dependences on experimental method, sample cell sealing and temperature, J. Phys. II 5(3) (1995) 413–425.
[151] P.M. Chaikin, T.C. Lubensky, Principles of Condensed Matter Physics, Cambridge University Press, Cambridge, UK, 2000.
[152] P.B. Canham, The minimum energy of bending as a possible explanation of the biconcave shape of the human red blood cell, J. Theor. Biol. 26(1) (1970) 61–81.
[153] E.A. Evans, Bending resistance and chemically induced moments in membrane bilayers, Biophys. J. 14(12) (1974) 923–931.
[154] P. Méléard, Elasticité de courbure de la bicouche lipidique: analyses statistique et dynamique des fluctuations thermiques de vésicules géantes, Ph.D. Thesis, Université de Bordeaux I, 1990.
[155] S.T. Milner, S.A. Safran, Dynamical fluctuations of droplet microemulsions and vesicles, Phys. Rev. A 36(9) (1987) 4371–4379.
[156] A.C. Rowat, P.L. Hansen, J.H. Ipsen, Experimental evidence of the electrostatic contribution to membrane bending rigidity, Europhys. Lett. 67 (2004) 144–149.
[157] G.B. Arfken, H.J. Weber, Mathematical Methods for Physicists, Academic press, New York, 2001.
[158] A.G. Petrov, I. Bivas, Elastic and flexoelectric aspects of out-of-plane fluctuations in biological and model membranes, Prog. Surface Sci. 16(4) (1984) 389–511.
[159] I. Szleifer, D. Kramer, A. Ben-Shaul, W.M. Gelbart, S.A. Safran, Molecular theory of curvature elasticity in surfactant films, J. Chem. Phys. 92 (1990) 6800.

[160] I. Szleifer, D. Kramer, A. Ben-Shaul, D. Roux, W.M. Gelbart, Curvature elasticity of pure and mixed surfactant films, Phys. Rev. Lett. 60(19) (1988) 1966–1969.
[161] J.R. Henriksen, A.C. Rowat, E. Brief, Y.W. Hsueh, J.L. Thewalt, M.J. Zuckermann, et al.Universal behavior of membranes with sterols, Biophys. J. 90(5) (2006) 1639–1649.
[162] J. Song, R.E. Waugh, Bilayer membrane bending stiffness by tether formation from mixed PC-PS lipid vesicles, J. Biomech. Eng. 112 (1990) 235.
[163] E. Andelmann, Electrostatics properties of membranes: the Poisson-Boltzmann theory, in: R. Lipowsky, E. Sackmann (Eds.), Handbook of Biological Physics vol. 1A Elsevier Science B.V, Amsterdam, Chapter 12, 1995.
[164] A. Fogden, B.W. Ninham, Electrostatics of curved fluid membranes: the interplay of direct interactions and fluctuations in charged lamellar phases, Adv. Colloid Interface Sci. 83(1–3) (1999) 85–110.